PFC/JA-83-18

RESONANT HELICALLY DISTORTED RELATIVISTIC ELECTRON BEAM EQUILIBRIA FOR FREE ELECTRON LASER APPLICATIONS

George L. Johnston
Ronald C. Davidson

Plasma Fusion Center
Massachusetts Institute of Technology
Cambridge, Massachusetts 02139

April, 1983

RESONANT HELICALLY DISTORTED RELATIVISTIC ELECTRON BEAM EQUILIBRIA FOR FREE ELECTRON LASER APPLICATIONS

George L. Johnston

and

Ronald C. Davidson

Plasma Fusion Center

Massachusetts Institute of Technology

Cambridge, Massachusetts 02139

ABSTRACT

This paper extends the development of a self-consistent kinetic description of helically distorted relativistic electron beam equilibria for free electron laser applications to include particular conditions of beam propagation, not treated heretofore, which are of considerable practical interest. Radially confined equilibria are considered for a helically distorted electron beam propagating in the combined transverse wiggler and uniform axial guide fields described by $\boldsymbol{B}^0 = B_0\hat{\boldsymbol{e}}_z + \delta\boldsymbol{B} = B_0\hat{\boldsymbol{e}}_z - \delta B\cos k_0 z\hat{\boldsymbol{e}}_x - \delta B\sin k_0 z\hat{\boldsymbol{e}}_y$, where $B_0 =$ const., $\delta B =$ const., and $\lambda_0 = 2\pi/k_0 =$ const. is the axial wavelength of the wiggler field. It is assumed that the beam density and current are sufficiently small that the equilibrium self fields can be neglected in comparison with $\boldsymbol{B}^0$. In this context, it is found that there are three useful (and exact) invariants $(C_\perp, C_h, C_z)$ associated with single-particle motion in the equilibrium field $B_0\hat{\boldsymbol{e}}_z + \delta\boldsymbol{B}$. These invariants are used to construct radially confined Vlasov equilibria $F_b^0(C_\perp, C_h, C_z)$ for an intense relativistic electron beam propagating in the z-direction. Examples of both solid and hollow beam equilibria are considered, and it is shown that the transverse wiggler field can have a large modulational influence on the beam envelope, depending on the size of $\delta B/B_0$ and other parameters. In the present work, no a priori assumption is made that the gyrofrequency $(\omega_c = eB_0/\gamma_b mc)$ of electron motion in the guide field and the frequency of axial electron motion $(\omega_0 = k_0 V_b)$ in the wiggler field are well separated. Thus the condition of beam-cyclotron resonance with $\omega_0 \simeq \omega_c$ can be treated. Numerical procedures for the determination of boundaries of both solid and hollow beam equilibria are developed, and calculations of solid and hollow beam boundaries at resonance are presented.

I. INTRODUCTION

There have been several theoretical [1—5] and experimental [6,7] investigations of the free electron laser which generates coherent electromagnetic radiation using an intense relativistic electron beam as an energy source. With few exceptions, theoretical studies of the free electron laser instability are based on highly simplified models which neglect the influence of finite radial geometry and beam kinetic effects, or make use of very idealized approximations in analyzing the matrix dispersion equation. The purpose of this paper is to extend the earlier development by Davidson and Uhm [8] of a self-consistent kinetic description of helically distorted relativistic electron beam equilibria for free electron laser applications to include particular conditions of beam propagation, not treated heretofore, which are of considerable practical interest.[9—14] In Ref. 8, Davidson and Uhm considered radially confined Vlasov equilibria for a helically distorted relativistic electron beam propagating in the combined transverse wiggler and uniform axial guide fields described by [Eqs. (1) and (2)]

$$\begin{aligned} \boldsymbol{B}^0 &= B_0\hat{\boldsymbol{e}}_z + \delta\boldsymbol{B} \\ &= B_0\hat{\boldsymbol{e}}_z - \delta B\cos k_0 z\hat{\boldsymbol{e}}_x - \delta B\sin k_0 z\hat{\boldsymbol{e}}_y, \end{aligned}$$

where $B_0 = \text{const.}$, $\delta B = \text{const.}$, and $\lambda_0 = 2\pi/k_0 = \text{const.}$ is the axial wavelength of the helical wiggler field. Both solid and hollow beam equilibria were considered, and it was assumed that the beam density and current are sufficiently small that equilibrium self fields can be neglected in comparison with $\boldsymbol{B}_0$. Within the context of this assumption it was found that there are three useful (and exact) invariants $(C_\perp, C_h, C_z)$ associated with single-particle motion in the equilibrium field $B_0\hat{\boldsymbol{e}}_z + \delta\boldsymbol{B}$. These invariants can be used to construct radially confined Vlasov equilibria $f_b^0(C_\perp, C_h, C_z)$ for an intense relativistic electron beam propagating in the z-direction, including the important modulational influence of the transverse wiggler field on the beam envelope. In the present work, we remove the restriction imposed in Ref. 8 that the gyrofrequency ($\omega_c = eB_0/\gamma_b mc$) of electron motion in the guide field and the frequency of axial electron motion ($\omega_0 = k_0 V_b$) in the wiggler field are well separated. The use of this restriction in Ref. 8 made it possible to obtain approximate analytic expressions for the beam boundaries. Its removal permits the treatment of the condition of beam-cyclotron resonance, in which $\omega_0 \simeq \omega_c$. Numerical procedures for the determination of boundaries of both solid and hollow beam equilibria are developed, and calculations of solid and hollow beam boundaries at resonance are presented.

In the process of extending the work of Ref. 8, it is necessary to redefine one of the invariants in order to consider beam equilibria near resonance. Accordingly, in the present analysis, we denote by C_z the redefined

axial invariant, and by C_z^0 the axial invariant defined in Ref. 8. The three exact invariants defined in Ref. 8 (modified as stated above) are given by the perpendicular invariant $C_\perp$ [Eq.(4)],

$$C_\perp = p_r^2 + p_\theta^2 + \frac{2eB_0}{ck_0}(p_z - \gamma_b m V_b) + \frac{2e}{ck_0}\boldsymbol{p}_\perp \cdot \delta\boldsymbol{B},$$

the helical invariant C_h [Eq.(5)],

$$C_h = P_\theta + \frac{1}{k_0}(p_z - \gamma_b m V_b) + \frac{e\delta B}{ck_0} r \sin(\theta - k_0 z),$$

and the axial invariant C_z [Eq.(6)],

$$C_z = \left(p_z - \frac{eB_0}{ck_0}\right)^2 - \frac{2e}{ck_0}\boldsymbol{p}_\perp \cdot \delta\boldsymbol{B},$$

where $\boldsymbol{p} = (p_r, p_\theta, p_z) = \gamma m \boldsymbol{v}$ is the mechanical momentum, $P_\theta = r(p_\theta - eB_0 r/2c)$ is the canonical angular momentum, $\gamma_b mc^2 =$ const. is the characteristic directed energy of the electron beam, and $V_b =$ const. is the characteristic mean axial velocity. In the expressions for $C_\perp$ and C_h, we have subtracted the constant terms proportional to $\gamma_b m V_b$ without loss of generality. Moreover, for $\delta\boldsymbol{B} = 0$, we note from Eq.(6) that the axial momentum p_z is a constant of the motion, and that Eqs. (4) and (5) yield the familiar invariants, $p_r^2 + p_\theta^2 =$ const. and $P_\theta =$ const., for a charged particle moving in a uniform axial field B_0.

The axial invariant C_z^0 defined in Ref. 8 is related to the axial invariant defined in the present work by $C_z = (C_z^0 - eB_0/ck_0)^2$. The definition of C_z^0 in Ref. 8 suggests erroneously that the right-hand side of Eq.(6) is restricted to non-negative values. By adding the axial and transverse invariant equations and moving all constants to one side of the resulting equation, one obtains the energy invariant

$$p_r^2 + p_\theta^2 + p_z^2 = p_0^2 = \text{const.},$$

where p_0^2 is defined by

$$p_0^2 = C_\perp + C_z - \frac{eB_0}{ck_0}\left(\frac{eB_0}{ck_0} - 2\gamma_b m V_b\right).$$

The energy invariant of course also follows directly from the equations of motion. We see that the only restriction is that p_0^2 be non-negative. If C_z is non-negative and equal to $(C_z^0 - eB_0/ck_0)^2$, and if in addition C_z^0 is set equal to $\gamma_b m V_b$, which is a condition imposed by the form of the distribution functions considered in Ref. 8, then $p_0^2 = C_\perp + (\gamma_b m V_b)^2$. The essence of the non-resonant approximation made in Ref. 8 is that the second term on the right-hand side of Eq.(6) is small compared with the first term. In that case, C_z is clearly positive.

In the present work we consider the approach to beam-cyclotron resonance ($C_z = 0$) through positive values of C_z. Thus the relation between C_z and C_z^0 stated above will be used. The necessity of redefining the axial invariant arises here because the moments of the distribution functions considered in Ref. 8 vanish as $\gamma_b m V_b \to eB_0/ck_0$, the condition for resonance.

The striking feature of the present analysis and that of Ref. 8 is the fact that the exact invariants $(C_\perp, C_h, C_z)$ can be used to construct helically distorted relativistic electron beam equilibria $f_b^0(C_\perp, C_h, C_z)$ of experimental interest for free electron laser applications. Generally speaking, the two classes of relevant beam equilibria can be characterized as: (a) solid beam equilibria, and (b) hollow beam equilibria. For example, equilibrium distribution functions of the form [Eq.(10)]

$$f_b^0 = F_1(C_\perp - 2\gamma_b m\omega_b C_h)G(C_z),$$

where $G(C_z)$ is a strongly peaked function of C_z, correspond to a solid electron beam with non-zero density on axis ($r = 0$). On the other hand, the class of beam equilibria described by [Eq.(11)]

$$f_b^0 = F_2(C_\perp)\delta(C_h - C_0)G(C_z),$$

where $C_0 = -(eB_0/2c)R_0^2 = \text{const.}$, corresponds to a slowly rotating annular electron beam with characteristic mean radius R_0. Of course, it is found that the detailed spatial dependence of beam equilibrium properties (density profile, temperature profile, etc.) depends on the specific functional form of $G(C_z), F_2(C_\perp)$ and $F_1(C_\perp - 2\gamma_b m\omega_b C_h)$. It is also found that the radial envelope of the beam can be strongly modulated by the transverse wiggler field, depending on the size of $\delta B/B_0$.

As a general remark, one of the most appealing features of the recent free electron laser stability analyses by Davidson and Uhm,[3] Sprangle and Smith, [5] and Bernstein and Hirshfield [4] for a relativistic electron beam with uniform density and infinite cross-section is the fact that the influence of the transverse wiggler field is contained in a fully self-consistent manner in the equilibrium distribution function $F_b^0 = n_0\delta(P_x)\delta(P_y)G_0(p_z)$. That is, when carrying out the stability analysis, the excited electromagnetic and electrostatic fields are treated as small-amplitude perturbations about a self-consistent equilibrium that includes the full nonlinear influence of the equilibrium wiggler field. We believe that the present equilibrium investigations and those in Ref. 8 form an important first step in formulating a self-consistent Vlasov description of the free electron laser instability that includes the effects of finite radial geometry and also correctly incorporates the nonlinear influence of the transverse wiggler field on the beam equilibrium.

The organization of this paper is the following. In Sec. II, we discuss the basic equilibrium configuration and assumptions. Specific examples of helically modulated relativistic electron beam equilibria are analyzed in

Sec. III, both for solid [Sec. III.A] and hollow [Sec. III.B] electron beams.

II. EQUILIBRIUM CONFIGURATION AND BASIC ASSUMPTIONS

We consider the class of helically modulated relativistic electron beam equilibria propagating in an externally applied magnetic field

$$\boldsymbol{B}^0 = B_0\hat{\boldsymbol{e}}_z + \delta\boldsymbol{B}, \tag{1}$$

where $B_0 = $ const. is the axial magnetic field, and

$$\delta\boldsymbol{B} = -\delta B\cos k_0 z\hat{\boldsymbol{e}}_x - \delta B\sin k_0 z\hat{\boldsymbol{e}}_y, \tag{2}$$

is the transverse helical wiggler field with axial wavelength $\lambda_0 = 2\pi/k_0$. In the present analysis, we assume that $\delta B = $ const. is a good approximation over the radial extent of the beam. In cylindrical polar coordinates (r,θ,z), Eq.(2) can also be expressed as

$$\begin{aligned}\delta\boldsymbol{B} &= \delta B_r\hat{\boldsymbol{e}}_r + \delta B_\theta\hat{\boldsymbol{e}}_\theta \\ &= -\delta B\cos(\theta - k_0 z)\hat{\boldsymbol{e}}_r + \delta B\sin(\theta - k_0 z)\hat{\boldsymbol{e}}_\theta,\end{aligned} \tag{3}$$

where $\hat{\boldsymbol{e}}_r$ and $\hat{\boldsymbol{e}}_\theta$ are unit vectors in the r- and θ-directions, respectively. It is assumed that the beam density and current are sufficiently low that the influence of the equilibrium self electric and self magnetic fields, $\boldsymbol{E}_s^0(\boldsymbol{x})$ and $\boldsymbol{B}_s^0(\boldsymbol{x})$, on the particle trajectories can be neglected in comparison with the $\boldsymbol{v}\times\boldsymbol{B}^0$ force associated with the applied magnetic field in Eq.(1).[15]

Within the context of the above assumptions, there are three useful and exact invariants $(C_\perp, C_h, C_z)$ associated with single-particle motion in the equilibrium field $B_0\hat{\boldsymbol{e}}_z + \delta\boldsymbol{B}$. These invariants can be used to construct cylindrical Vlasov equilibria $F_b^0(C_\perp, C_h, C_z)$ for an intense relativistic electron beam propagating in the z-direction, including the important modulational influence of the transverse wiggler field on the beam envelope. For relativistic electron motion in the applied magnetic field defined in Eqs. (1) and (2), the three exact invariants are given by [8] the transverse invariant $C_\perp$

$$C_\perp = p_r^2 + p_\theta^2 + \frac{2eB_0}{ck_0}(p_z - \gamma_b m V_b) + \frac{2e}{ck_0}\boldsymbol{p}_\perp\cdot\delta\boldsymbol{B}, \tag{4}$$

the helical invariant C_h

$$C_h = P_\theta + \frac{1}{k_0}(p_z - \gamma_b m V_b) + \frac{e\delta B}{ck_0} r \sin(\theta - k_0 z), \tag{5}$$

and the axial invariant C_z

$$C_z = \left(p_z - \frac{eB_0}{ck_0}\right)^2 - \frac{2e}{ck_0} \boldsymbol{p}_\perp \cdot \delta \boldsymbol{B}. \tag{6}$$

In Eqs. (4)-(6), $\boldsymbol{p} = (p_r, p_\theta, p_z) = \gamma m \boldsymbol{v}$ is the mechanical momentum, $P_\theta = r(p_\theta - eB_0 r/2c)$ is the canonical angular momentum associated with the axial field B_0, $\gamma mc^2 = (m^2c^4 + c^2p^2)^{\frac{1}{2}}$ is the relativistic electron energy, $-e$ is the electron charge, m is the electron rest mass, $\gamma_b mc^2 =$ const. is the characteristic directed energy of the electron beam, and $V_b =$ const. is the characteristic mean axial velocity. Moreover, $\boldsymbol{p}_\perp$ is the transverse momentum, and $\boldsymbol{p}_\perp \cdot \delta \boldsymbol{B}$ can be expressed as $\boldsymbol{p}_\perp \cdot \delta \boldsymbol{B} = -p_r \delta B \cos(\theta - k_0 z) + p_\theta \delta B \sin(\theta - k_0 z)$. Note in Eqs. (4) and (5) that we have subtracted the constant terms proportional to $\gamma_b m V_b$ without loss of generality. For $B_0 =$ const. and $\delta B =$ const., we reiterate that $C_\perp, C_h$ and C_z are *exact* constants of the motion for arbitrary wiggler amplitude δB.

In the limit of zero wiggler amplitude, $\delta B \to 0$, Eqs. (4)-(6) reduce to

$$C_\perp = p_r^2 + p_\theta^2 + \frac{2eB_0}{ck_0}(p_z - \gamma_b m V_b) = \text{const.}, \tag{7}$$

$$C_h = P_\theta + \frac{1}{k_0}(p_z - \gamma_b m V_b) = \text{const.}, \tag{8}$$

$$C_z = \left(p_z - \frac{eB_0}{ck_0}\right)^2 = \text{const.} \tag{9}$$

For $\delta B = 0$, we note from Eq.(9) that the axial momentum p_z is a constant of the motion, and Eqs. (7) and (8) yield the familiar invariants, $p_r^2 + p_\theta^2 =$ const. and $P_\theta =$ const., for a charged particle moving in a uniform axial field B_0.

There are two classes of helical beam equilibria $F_b^0(C_\perp, C_h, C_z)$ of experimental interest for free electron laser applications. Generally speaking, the two classes can be characterized as: (a) solid beam equilibria, and (b) hollow beam equilibria. For example, equilibrium distribution functions of the form

$$f_b^0 = F_1(C_\perp - 2\gamma_b m \omega_b C_h) G(C_z), \tag{10}$$

where $G(C_z)$ is a strongly peaked function of C_z, corresponds to a solid electron beam with non-zero density on axis ($r = 0$). In Eq.(10), $\omega_b =$ const. is related to the mean angular rotation of the beam [Sec. III]. On the other hand, the class of beam equilibria described by

$$f_b^0 = F_2(C_\perp)\delta(C_h - C_0)G(C_z), \tag{11}$$

where $C_0 = -(eB_0/2c)R_0^2 = \text{const.}$, corresponds to a slowly rotating annular electron beam with characteristic mean radius R_0. The corresponding distribution functions considered in Ref. 8 differ from those of Eqs. (10) and (11) in that, instead of $G(C_z)$, they contain a function of C_z^0 which is strongly peaked around $C_z^0 = C_{z0}$, where $C_{z0} = \gamma_b m V_b$. We shall henceforth denote this function by $G^0(C_z^0)$. Of course, the detailed spatial dependence of the beam equilibrium properties (e.g., density profile, temperature profile, etc.) depends on the specific functional form of $G(C_z)$, $F_1(C_\perp - 2\gamma_b m\omega_b C_h)$ and $F_2(C_\perp)$. In this regard, specific examples of helical beam equilibria are discussed in Sec. III. As a general remark, it is found that the radial extent of the beam can be strongly modulated by the transverse wiggler field, depending on the size of $\delta B/B_0$ and other parameters.

While it is true that beam equilibrium properties can be calculated making use of the exact invariants in Eqs. (4)-(6), there are useful approximations that can sometimes be made in simplifying the expression for C_z [Eq.(6)] in some regimes of practical interest for free electron laser applications. We now discuss these approximations, which are used in the detailed equilibrium examples presented in Ref. 8. First, in some regimes of practical interest, the characteristic transverse momentum $\boldsymbol{p}_\perp$ of a beam electron is small in comparison with the characteristic directed axial momentum $\gamma_b m V_b \simeq p_z$, i.e.,

$$|\boldsymbol{p}_\perp| \ll \gamma_b m V_b. \tag{12}$$

Second,it is assumed in the detailed equilibrium examples presented in Ref. 8 that the beam axial motion is far removed from cyclotron resonance. Specifically, referring to Eq.(6), it is assumed that

$$\left|\gamma_b m V_b - \frac{eB_0}{ck_0}\right|^2 \gg \frac{2e}{ck_0}|\boldsymbol{p}_\perp \cdot \delta\boldsymbol{B}|, \tag{13}$$

or equivalently,

$$|\omega_0 - \omega_c|^2 \gg 2\omega_c\omega_0\left|\frac{\boldsymbol{p}_\perp}{\gamma_b m V_b} \cdot \frac{\delta\boldsymbol{B}}{B_0}\right|, \tag{14}$$

where ω_0 and ω_c are defined by

$$\omega_0 = k_0 V_b \quad \text{and} \quad \omega_c = \frac{eB_0}{\gamma_b mc}. \tag{15}$$

To assure radial confinement of the beam electrons, the analysis of course assumes $B_0 \neq 0$. Making use of the inequality $|\boldsymbol{p}_\perp| \ll \gamma_b m V_b$ [Eq.(12)], the striking feature of that analysis is that the inequality in Eq.(14) is easily

satisfied even for large wiggler amplitude ($\delta B \approx B_0$, say), both in the limits of weak axial field ($\omega_c^2 \ll \omega_0^2$) and strong axial field ($\omega_c^2 \gg \omega_0^2$). For example, if $\omega_0^2 \gg \omega_c^2$, then Eq.(14) reduces to

$$1 \gg 2\frac{\omega_c}{\omega_0}\left|\frac{\boldsymbol{p}_\perp}{\gamma_b m V_b}\cdot\frac{\delta \boldsymbol{B}}{B_0}\right|, \tag{16}$$

which is readily satisfied in some parameter regimes of experimental interest. In any case, within the context of the inequalities in Eqs. (12) and (13), the exact axial invariant C_z^0, defined in Ref. 8, can be approximated by

$$C_z^0 = p_z - \frac{e}{ck_0}\frac{\boldsymbol{p}_\perp \cdot \delta \boldsymbol{B}}{(p_z - eB_0/ck_0)} \tag{17}$$

where we have taken the positive square root in Eq.(6), which corresponds to C_z^0 and p_z having the same polarity. Equation (17) is an excellent approximation to C_z^0 in some parameter regimes of practical interest for free electron laser applications. Moreover, for $G^0(C_z^0)$ strongly peaked about $C_z^0 = \gamma_b m V_b$, with characteristic half-width $\Delta C_z^0 \ll \gamma_b m V_b$, the denominator on the right-hand side of Eq.(17) can be approximated by $p_z - eB_0/ck_0 = \gamma_b m V_b - eB_0/ck_0$. Equation (17) then reduces to

$$C_z^0 = p_z - \frac{\omega_c}{\omega_0 - \omega_c}\boldsymbol{p}_\perp \cdot \frac{\delta \boldsymbol{B}}{B_0}, \tag{18}$$

which is the approximate form of the axial invariant used in Ref. 8. [Recall that the axial invariant defined in Ref. 8, namely C_z^0, is related to the axial invariant defined in the present work by the relation $C_z = (C_z^0 - eB_0/ck_0)^2$.]

In the present work we remove the restriction of Ref. 8 that the axial invariant equation, Eq.(6), be approximated by its nonresonant approximation, Eq.(18). Thus we are able to consider the behavior of beam equilibria near resonance ($\omega_0 \simeq \omega_c$). We will find in the next section that the functional forms of beam equilibria considered will have to be modified from those of Ref. 8 in order to ensure that the beam particle density does not vanish at resonance.

III. EXAMPLES OF HELICALLY MODULATED RELATIVISTIC ELECTRON BEAM EQUILIBRIA

There is clearly a wide variety of helically modulated relativistic electron beam equilibria that can be analyzed within the context of the equilibrium formalism described in Sec. II. The relevant choice of $f_b^0(C_\perp, C_h, C_z)$ of course depends in detail on injection geometry, beam quality, etc. For our purposes here, we consider two simple examples of solid and hollow beam equilibria that clearly illustrate the strong influence of the transverse wiggler field in modulating the beam envelope. In both cases, for simplicity, it is assumed that the axial distribution $G(C_z)$ is cold,

$$G(C_z) = \delta(C_z - C_{z0}), \tag{19}$$

where C_{z0} is a constant. When C_{z0} is non-negative, we equate it to the quantity $(\gamma_b m V_b - eB_0/ck_0)^2$. This ensures that $p_r^2 + p_\theta^2 + p_z^2 = C_\perp + (\gamma_b m V_b)^2$. In Ref. 8, the equilibria involve, instead of the function of the axial invariant given in Eq.(19), the function

$$G^0(C_z^0) = \delta(C_z^0 - \gamma_b m V_b). \tag{20}$$

In the present work we introduce the notation G^0 to emphasize the difference between the two functions. The functional form of Eq.(20) is inappropriate for conditions near resonance because the equilibrium density profiles near resonance are proportional to $[\gamma_b m V_b - (eB_0/ck_0)]$ and thus vanish at resonance. We can easily see this by considering the identity

$$\delta[f(x)] = \sum_{\{n\}} \frac{\delta(x - x_n)}{|f'(x_n)|}, \tag{21}$$

in which the x_n are the zeros of $f(x)$. The partial derivatives of C_z^0 with respect to components of momentum are proportional to $[\gamma_b m V_b - (eB_0/ck_0)]^{-1}$. In performing the integral with respect to momentum of an equilibrium distribution function in which $G^0(C_z) = \delta(C_z^0 - \gamma_b m V_b)$, we obtain a factor $[\gamma_b m V_b - (eB_0/ck_0)]$. The partial derivatives of the argument of the delta-function in Eq.(19) with respect to components of momentum are not proportional to $[\gamma_b m V_b - (eB_0/ck_0)]^{-1}$ and thus do not vanish at resonance. We also note that although the moments of corresponding distribution functions in Ref. 8 and in the present work differ, the beam boundaries do not differ.

A. *Solid Beam Equilibria*

As an example of a helically modulated *solid* electron beam, consider the case where $f_b^0(C_\perp, C_h, C_z)$ has the form [Eq. (10)]

$$f_b^0 = N_s\delta(C_\perp - 2\gamma_b m\omega_b C_h - 2\gamma_b m\hat{T}_\perp)\delta(C_z - C_{z0}), \tag{22}$$

where $C_\perp$ and C_h are defined in Eqs. (4) and (5), C_z is defined in Eq.(6), and N_s, ω_b and $\hat{T}_\perp$ are positive constants. Note that the dimensions of the normalization constant are those of particle density times momentum. Equation (22) is a straightforward generalization of the uniform density beam equilibria $f_b^0 = (n_0/\pi)\delta(p_r^2 + p_\theta^2 - 2\gamma_b m\omega_b P_\theta - 2\gamma_b m\hat{T}_\perp)\delta(p_z - \gamma_b m V_b)$ previously discussed by Davidson [15] for the case $\delta B = 0$ and $f_b^0 = (n_0/\pi)\delta(C_\perp - 2\gamma_b m\omega_b C_h - 2\gamma_b m\hat{T}_\perp)\delta(C_z^0 - \gamma_b m V_b)$ previously considered by Davidson and Uhm [8] for the nonresonant case with $\delta B \neq 0$.

Before proceeding further, we note that the axial invariant equation [Eq.(6)] does not depend on the component of transverse momentum perpendicular to $\delta\boldsymbol{B}$. It will prove convenient in the case of solid beam equilibria to exploit this fact by introducing a particular transformation of momentum variables. We denote by p_1 the component of momentum parallel to $\delta\boldsymbol{B}$. The transformation which we consider is $(p_r, p_\theta, p_z) \rightarrow (p_1, p_2, p_z)$, where (p_1, p_2, p_z) forms a right-handed coordinate system. The relations between the original and transformed transverse momentum components are

$$p_r = -\cos(\theta - k_0 z)p_1 - \sin(\theta - k_0 z)p_2, \tag{23}$$

$$p_\theta = \sin(\theta - k_0 z)p_1 - \cos(\theta - k_0 z)p_2. \tag{24}$$

We denote the argument of the first delta-function in Eq.(22) by $(C_\perp - 2\gamma_b m\omega_b C_h - 2\gamma_b m\hat{T}_\perp) = K$. Introducing the transformation of momentum variables discussed above, and defining $2\hat{T}_\perp/\gamma_b m \equiv v_0^2$ then gives

$$\begin{aligned} K(p_1, p_2, p_z) &= p_1^2 + p_2^2 + p_z^2 \\ &\quad - \frac{2\gamma_b m\omega_b}{k_0}\Big\{ (k_0 r)\big[\sin(\theta - k_0 z)p_1 - \cos(\theta - k_0 z)p_z \\ &\quad - (eB_0/2ck_0)(k_0 r)\big] + (p_z - \gamma_b m V_b) + \frac{e\delta B}{ck_0}(k_0 r)\sin(\theta - k_0 z)\Big\} \\ &\quad - \big[(\gamma_b m v_0)^2 + (\gamma_b m V_b)^2\big]. \end{aligned} \tag{25}$$

We now evaluate various macroscopic properties of physical interest for the choice of distribution function in Eq.(22). Consider the equilibrium density profile $n_b^0(r, \theta, z) = \int d^3p f_b^0(C_\perp, C_h, C_z)$. Equation (22) gives

$$n_b^0(r,\theta - k_0 z) = N_s \int dp_1 dp_2 dp_z \delta(K)\delta(C_z - C_{z0}), \tag{26}$$

where K is defined in Eq.(25). Since the axial invariant equation [Eq.(6)] and therefore the argument of the second delta function in Eq.(26), do not depend on p_2, it is convenient to perform the integration with respect to p_2 first. The quantity K can be expressed in the form

$$K = (p_2 - p_{20})^2 - \sigma, \tag{27}$$

where $p_{20} = (\gamma_b m \omega_b / k_0)\cos(\theta - k_0 z) k_0 r$ and σ is independent of p_2. The condition $K = 0$ implies

$$(p_2 - p_{20})^2 = \sigma, \tag{28}$$

where σ is required to be non-negative. We denote the values of p_2 which satisfy Eq.(28) by $p_2^{\pm}$, i.e.,

$$p_2^{\pm} = p_{20} \pm \sigma^{\frac{1}{2}}. \tag{29}$$

Therefore, $\delta(K)$ can be expressed in the form

$$\delta(K) = \left[\frac{\delta(p_2 - p_2^+)}{|\partial K/\partial p_2|_{p_2^+}} + \frac{\delta(p_2 - p_2^-)}{|\partial K/\partial p_2|_{p_2^-}}\right] u(\sigma), \tag{30}$$

where u is the unit step function. Evaluation of the partial derivatives of K in Eq.(30) gives

$$\delta(K) = \frac{[\delta(p_2 - p_2^+) + \delta(p_2 - p_2^-)]}{2\sigma^{\frac{1}{2}}} u(\sigma). \tag{31}$$

Introducing this representation of $\delta(K)$ into Eq.(26), and performing the integration with respect to p_2, we find

$$n_b^0(r,\theta - k_0 z) = N_s \int dp_1 dp_z \frac{\delta(C_z - C_{z0})}{\sigma^{\frac{1}{2}}} u(\sigma). \tag{32}$$

The integration with respect to p_1 is performed next. The reason for this order of integration is that the form of the axial invariant equation [Eq.(6)] is such that p_1 is a single-valued function of p_z, but the converse is not true. This consideration becomes important as the condition of beam-cyclotron resonance is approached because the axial invariant surface can no longer be approximated by a plane tangent to the axial invariant surface at $p_1 = 0$, as is done in the nonresonant approximation. We can express the delta function in Eq.(32) in the form

$$\delta(C_z - C_{z0}) = \frac{\delta(p_1 - \tilde{p}_1)}{|\partial C_z/\partial p_1|_{\tilde{p}_1}}, \tag{33}$$

where $\tilde{p}_1$ denotes the function of p_z which is determined by the axial invariant equation [Eq.(6)] with the substitution $C_z = C_{z0} = (\gamma_b m V_b - eB_0/ck_0)^2$, i.e.,

$$\tilde{p}_1(p_z) = \frac{\left[(p_z - eB_0/ck_0)^2 - (\gamma_b m V_b - eB_0/ck_0)^2\right]}{(2e\delta B/ck_0)}. \tag{34}$$

Evaluating the partial derivative in Eq.(33), we obtain

$$\delta(C_z - C_{z0}) = \left(\frac{2e}{ck_0}\delta B\right)^{-1} \delta(p_1 - \tilde{p}_1). \tag{35}$$

Introducing this representation of $\delta(C_z - C_{z0})$ into Eq. (32) and performing the integration with respect to p_1, we obtain

$$n_b^0 = N_s\left(\frac{2e}{ck_0}\delta B\right)^{-1} \int dp_z \frac{u(\tilde{\sigma})}{\tilde{\sigma}^{\frac{1}{2}}}, \tag{36}$$

where the tilde on σ denotes the replacement of p_1 by $\tilde{p}_1(p_z)$ as given in Eq.(34).

The quantity $\tilde{\sigma}$ is a quadratic in $k_0 r$. It is convenient to express it in the form

$$\tilde{\sigma} = -[a(k_0 r)^2 + \tilde{b}(k_0 r) + \tilde{c}], \tag{37}$$

where

$$a = \frac{\gamma_b m\omega_b}{k_0}\left[\frac{eB_0}{ck_0} - \frac{\gamma_b m\omega_b}{k_0}\cos^2(\theta - k_0 z)\right], \tag{38}$$

$$\tilde{b} = -2\frac{\gamma_b m\omega_b}{k_0}\sin(\theta - k_0 z)\left[\tilde{p}_1(p_z) + \frac{e\delta B}{ck_0}\right], \tag{39}$$

$$\tilde{c} = [\tilde{p}_1(p_z)]^2 + p_z^2 - 2\frac{\gamma_b m\omega_b}{k_0}(p_z - \gamma_b m V_b) - (\gamma_b m v_0)^2 - (\gamma_b m V_b)^2. \tag{40}$$

To ensure that the quantity a given in Eq.(38) does not change sign as $(\theta - k_0 z)$ varies, we require that $eB_0/ck_0 > \gamma_b m\omega_b/k_0$, with the result that a is positive.

The function $k_0 r(p_z)$ determined by solution of the equation $\tilde{\sigma} = 0$ is of interest because the range of integration in the integral expression for the equilibrium density profile $n_b^0(r, \theta - k_0 z)$ [Eq.(36)] is determined by the condition $\tilde{\sigma} > 0$. The solution of the quadratic equation $\tilde{\sigma} = 0$ is

$$k_0 r(p_z) = -\frac{\tilde{b}}{2a} + \frac{1}{2a}(\tilde{b}^2 - 4a\tilde{c})^{\frac{1}{2}}. \tag{41}$$

We have chosen the positive sign in the quadratic formula because a is positive. Examination of Eq.(37), which gives $\tilde{\sigma}$ as a quadratic in $k_0 r$, indicates that $\tilde{\sigma} > 0$ for $0 \leq k_0 r < k_0 r(p_z)$ and that $\tilde{\sigma} < 0$ for $k_0 r(p_z) < k_0 r$.

The varieties of behavior of $k_0 r(p_z)$ which are significantly distinct are shown in Fig.1. As indicated above, the regions between the curves and the p_z–axis are regions in $(p_z, k_0 r)$ space in which $\tilde{\sigma} > 0$. The regions of p_z in which $k_0 r(p_z)$ is represented as having the value zero are regions in which $k_0 r(p_z)$ is complex. This occurs because the discriminant $d = (\tilde{b}^2 - 4a\tilde{c})$ in Eq.(41) is negative. The basis for the cutoff behavior of the curves in Fig. 1 is easily understood from an examination of the discriminant. We have

$$\begin{aligned} d = {} & 4\left(\frac{\gamma_b m\omega_b}{k_0}\right)^2 \sin^2(\theta - k_0 z)\left[\tilde{p}_1(p_z) + \frac{e\delta B}{ck_0}\right]^2 \\ & - 4\left(\frac{\gamma_b m\omega_b}{k_0}\right)\left[\frac{eB_0}{ck_0} - \frac{\gamma_b m\omega_b}{k_0}\cos^2(\theta - k_0 z)\right]\Big\{ [\tilde{p}_1(p_z)]^2 \\ & + p_z^2 - 2\frac{\gamma_b m\omega_b}{k_0}(p_z - \gamma_b m V_b) - (\gamma_b m v_0)^2 - (\gamma_b m V_b)^2\Big\} \end{aligned} \tag{42}$$

Note that the discriminant is a quartic in p_z. Thus the equation $d = 0$ can have four, two, or zero real roots. From Eq.(34) we see that, as $(p_z - eB_0/ck_0)^2$ assumes sufficiently large values, the terms in Eq.(42) which contain $\tilde{p}_1(p_z)$ become dominant and d becomes negative. The situation can be characterized by

$$d \to -4\left(\frac{\gamma_b m\omega_b}{k_0}\right)\left[\frac{eB_0}{ck_0} - \left(\frac{\gamma_b m\omega_b}{k_0}\right)\right][\tilde{p}_1(p_z)]^2 + \cdots. \tag{43}$$

for large $(p_z - eB_0/ck_0)^2$. This is the basis for the cutoff behavior of the curves of Fig.1 at the extreme values of p_z. To determine the basis for the occurrence (or non-occurrence) of cutoff behavior at intermediate values of p_z shown in Fig. 1(a), we again consider Eq.(34). The function $\tilde{p}_1(p_z)$ describes a right parabolic cylinder in momentum space whose generators are parallel to the p_2–axis. The minimum values of $\tilde{p}_1$ (achieved for $p_z = eB_0/ck_0$) is $\tilde{p}_1(eB_0/ck_0) = -(\gamma_b m V_b - eB_0/ck_0)^2/(2e\delta B/ck_0) = -[\gamma_b m V_b/(eB_0/ck_0) - 1]^2/(2\delta B/B_0)$. If this value is sufficiently large in magnitude, d will be negative within a singly connected region of values of p_z near eB_0/ck_0. Again, the situation can be characterized by Eq.(43). Thus, for suitable values of parameters, the equation $d = 0$ will have four real roots, and the cutoff behavior of $k_0 r(p_z)$ will be as shown in Fig. 1(a). If $\tilde{p}_1(eB_0/ck_0)$ is not sufficiently large in magnitude, this will not occur. For suitable values of the parameters, the equation $d = 0$ will have two real roots, and the cutoff behavior of $k_o r(p_z)$ will be as shown in Fig.1(b) and Fig. 1(c).

The magnitude of $\tilde{p}_1(eB_0/ck_0)$ stated above is a measure of the approach of the system to beam-cyclotron resonance. The expression for $\tilde{p}_1(eB_0/ck_0)$ can be rewritten as

$$\frac{\tilde{p}_1(eB_0/ck_0)}{eB_0/ck_0} = -\frac{\delta B}{B_0}\frac{[\gamma_b m V_b/(eB_0/ck_0) - 1]^2}{2(\delta B/B_0)^2}. \tag{44}$$

The condition for beam-cyclotron resonance is[9]

$$\frac{1}{2}\left(\frac{\gamma_b m V_b}{eB_0/ck_0} - 1\right)^2 \ll \left(\frac{\delta B}{B_0}\right)^2 \ll 1. \tag{45}$$

For experimental conditions of interest, $(\delta B/B_0) \lesssim 1/3$. Thus, by comparing Eqs.(44) and (45), we find for parameters sufficiently far from beam-cyclotron resonance, that there will be cutoff behavior at intermediate values of p_z, as indicated in Fig. 1(a). Otherwise, the situation will be as indicated in Figs. 1(b) or 1(c).

Having discussed the basis for the several varieties of cutoff behavior of $k_0 r(p_z)$, we now proceed to give prescriptions for the range of integration in the integral expression for $n_b^0(r, \theta - k_0 z)$ in Eq.(36) and the radial boundary of the electron beam. For particular values of $k_0 r$ and $(\theta - k_0 z)$, the range of integration in Eq.(36) is determined by the intersection of a horizontal line at the given value of $k_0 r$ with the regions between the curves and the p_z axis. This prescription is subject to the important restriction noted below.

The radial boundary of the electron beam, $R_b(\theta - k_0 z)$, is determined by solving numerically for the maximum value of $k_0 r(p_z)$, i.e.,

$$k_0 R_b = \max_{\{p_z\}}\{k_0 r(p_z)\}. \tag{46}$$

This prescription is also subject to the important restriction noted below.

The restrictions to the above prescriptions for determining the range of integration in $n_b^0(r, \theta - k_0 z)$ and the beam boundary R_b are now given. If for all values of $(\theta - k_0 z)$ the curve of $k_0 r(p_z)$ exhibits cutoff behavior for intermediate values of p_z [as shown in Fig.1(a)], then it is permissible to consider equilibrium distribution functions in which particles are present only in the larger (or smaller) simply-connected region of permitted values of p_z, instead of both ranges. The determination of the range of integration in $n_b^0(r, \theta - k_0 z)$ and the beam boundary R_b are then carried out without regard to the other range of values of p_z. Note that no distinction is made between the case of Fig. 1(b) and that of Fig. 1(c).

The justification for this exception is based upon consideration of the set of functions $k_0 r(p_z)$ corresponding to the entire range of values of $(\theta - k_0 z)$. Consider a particle orbit which passes through a particular phase point $(r, \theta - k_0 z, p_z)$. If for all values of $(\theta - k_0 z)$ the curve of $k_0 r(p_z)$ exhibits cutoff behavior for intermediate values of p_z [as shown in Fig. 1(a)], then the set of phase points corresponding to a given particle

orbit lies completely on one side of the intermediate cutoff region. Thus, elimination of particles in one simply-connected region of permitted values of p_z does not result in physically unrealistic truncation of any particle orbits.

Equilibrium distribution functions in which particles are present only in the large range of permitted values of p_z have particular physical significance. They correspond to an intense relativistic electron beam propagating primarily in the z direction which can be considered to evolve by adiabatic increase of δB from beams for which $\delta B = 0$ and all particles have $p_z = \gamma_b m V_b$.

The basis for the preceding assertions is now developed. In order to do so, it is necessary to consider the Duffing equation for p_z which is obtained from the single-particle equation of motion[9,16]

$$\frac{d^2\eta}{d\tau^2} + \frac{1}{2}\eta^3 + \left[\left(\frac{\delta B}{B_0}\right)^2 - \frac{1}{2}C_z^*\right]\eta + \left(\frac{\delta B}{B_0}\right)^2 = 0, \tag{47}$$

where $\eta = (k_0 v_z/\omega_{c0}) - 1 = [p_z/(eB_0/ck_0) - 1]$, $\tau = \omega_{c0}t$, $\omega_{c0} = eB_0/\gamma mc$, and the normalized invariant C_z^* is related to the axial invariant C_z by $C_z^* = (eB_0/ck_0)^{-2}C_z$. The first integral of the Duffing equation is

$$\frac{1}{2}\left(\frac{d\eta}{d\tau}\right)^2 + U(\eta) = 0, \tag{48}$$

The pseudopotential is $U(\eta) = V(\eta) + C$, where

$$V(\eta) = \frac{1}{8}\eta^4 + \frac{1}{2}\left[\left(\frac{\delta B}{B_0}\right)^2 - \frac{1}{2}C_z^*\right]\eta^2 + \left(\frac{\delta B}{B_0}\right)^2\eta, \tag{49}$$

and

$$C = \left[\frac{1}{8}C_z^{*2} + \frac{1}{2}\left(\frac{\delta B}{B_0}\right)^2(1 - p_0^{*2})\right]. \tag{50}$$

The normalized invariant p_0^* is related to the energy invariant $p_0 = (p_x^2 + p_y^2 + p_z^2)^{\frac{1}{2}}$ by $p_0^* = p_0/(eB_0/ck_0)$. Note that $p_0^* > 1$ since $\omega_c/\omega_0 = [(eB_0/\gamma_b mc)/k_0 V_b]$ is less than or equal to one for the cases considered here. This is significant because it ensures that the coefficient of $(\delta B/B_0)^2$ in the expression for C is negative. The allowed values of η (or equivalently p_z) for a particle correspond to negative values of $U(\eta)$. Consider the dependence of $V(\eta)$ and C on the dynamical invariants of the motion. The quantity $V(\eta)$, and therefore the shape of the pseudopotential $U(\eta)$, depends on the axial invariant. However, the value of the constant C, and therefore the vertical position of the pseudopotential curve in Fig. 2, depends on both the axial invariant and the energy invariant. Since the functional form of the solid beam equilibrium distribution function in Eq.(22) specifies a single value of the axial invariant, but does not specify a single value of the energy invariant, the

pseudopotential curves corresponding to Eq.(22) will all have the same shape but different vertical positions on the pseudopotential diagram.

Figure 2 shows a selection of pseudopotential curves which are significantly distinct from one another, and the associated phase space orbits in $(\eta, d\eta/d\tau)$ space. Figure 2(a) shows the case $\delta B = 0$, for which particles have two possible values of p_z, i.e., either $p_z = \gamma_b m V_b$ or $p_z = (2eB_0/ck_0 - \gamma_b m V_b)$. Note that in this singular case the shape of the pseudopotential curve is independent of the energy invariant. Figures 2(b)-(e) show a sequence of pseudopotential curves which correspond to an evolution toward beam-cyclotron resonance. Such a sequence can be produced by increasing $\delta B/B_0$, by reducing C_z^*, or by some combination of the two. In this regard, use is made of Eqs.(44), (49) and (50).

If and only if, for every particle in a given equilibrium distribution function, the pseudopotential curve is of the type shown in Fig. 2(b) [or, in Fig. 2(a), as $\delta B \to 0$], will the corresponding set of curves of $k_0 r(p_z)$ for all values of $(\theta - k_0 z)$ be of the type shown in Fig. 1(a). Since the two allowable regions of phase space are isolated from each other, it is permissible to consider distributions in which only one region of phase space, or one simply connected region of p_z in $k_0 r(p_z)$ contains particles. If the region of larger (smaller) values of p_z is occupied, then the limiting distribution as $\delta B \to 0$ is one in which all particles have $p_z = \gamma_b m V_b (2eB_0/ck_0 - \gamma_b m V_b)$.

As a numerical example, in Fig. 3 we show a plot of the normalized radius $k_0 R_b$ of the beam envelope [Eq.(47)] versus $(\theta - k_0 z)$ for several values of ω_c/ω_0 and the choice of equilibrium parameters $\delta B/B_0 = 0.01$, $V_b^2/c^2 = 8/9$, $v_0^2/c^2 = 0.02$, and $\omega_b = 0.75\omega_c$. The normalized radius is determined from Eq.(47), where $k_0 r(p_z)$ is calculated from Eq.(41) and Eqs.(38)–(40), subject to the restriction that if the curve of $k_0 r(p_z)$ exhibits the cutoff behavior indicated in Fig. 1(a), the range of values of p_z from which the maximum is chosen is limited to the singly–connected region of higher values of p_z. For cases where this restriction applies, the equilibrium distribution function can be considered to evolve by adiabatic increase of δB from beams for which $\delta B = 0$ and all particles have $p_z = \gamma_b m V_b$. For $\omega_c/\omega_0 = 0.8$ [Fig. 3(a)] and $\omega_c/\omega_0 = 0.9$ [Fig. 3(b)], the curve of $k_0 r(p_z)$ exhibits the cutoff behavior indicated in Fig. 1(a), and the restriction stated above is imposed. For $\omega_c/\omega_0 = 0.95$ [Fig. 3(c)] and $\omega_c/\omega_0 = 1.0$ [Fig. 3(d)], the curve $k_0 r(p_z)$ has real values only in one singly–connected region of p_z. The curve in Fig. 3(a) is approximated reasonably well by the approximate nonresonant analysis in Ref. 8. The curve in Fig. 3(b) exhibits substantial deviation from the results of the non-resonant approximation. Note in particular the difference between the portion of the curve in the range $0 \leq (\theta - k_0 z) < \pi$ and that in the range $\pi \leq (\theta - k_0 z) < 2\pi$. For ω_c/ω_0 in the range between 0.9 and 0.95, there is a transition in which the curve for $k_0 r(p_z)$ exhibits the cutoff behavior in Fig. 3(a) for some values of $(\theta - k_0 z)$ and that in Fig. 3(b) or Fig. 3(c) for other values of $(\theta - k_0 z)$. The curves in Fig. 3(c) and Fig. 3(d)

exhibit a reversal, relative to the curves of Fig. 3(a) and Fig. 3(b), of the region of $(\theta - k_0 z)$ in which the value of $k_0 R_b$ is larger than its value at $(\theta - k_0 z) = 0, \pi$, and that in which the value is smaller. The curves in Fig. 3(c) and Fig. 3(d) cannot be approximated by the nonresonant analysis of Ref. 8. In comparing the curves in Fig. 3 with those in Fig. 1 of Ref. 8, note that there is a sign error in the latter curves which results from the omission [in Eq.(30) of Ref. 8] of a minus sign preceding the term $\Delta R_b \sin(\theta - k_0 z)$.

We conclude this section by emphasizing that the theoretical analysis developed here can be used to calculate the equilibrium properties of a helically modulated solid electron beam propagating in an equilibrium magnetic field prescribed by Eqs.(1) and (2) without imposing any approximations other than those implicit in the magnetic field configuration assumed.

B. Annular Electron Beam

As an example of a helically modulated *annular* electron beam, we consider the case where $f_b^0(C_\perp, C_h, C_z)$ has the form [cf. Eq. (11)]

$$f_b^0 = N_s \delta(C_\perp - \gamma_b^2 m^2 v_0^2) \times \delta(C_h - C_0)\delta(C_z - C_{z0}), \tag{51}$$

where $C_0 = -eB_0 R_0^2/2c = \text{const.}$, and N_s is a positive constant. This distribution function is similar to the annular beam equilibrium distribution function considered in Ref. 8. The principal difference is the form of the factor containing the axial invariant, i.e., $\delta(C_z - C_{z0})$ instead of $\delta(C_z^0 - \gamma_b m V_b)$. The development of expressions for moments of the distribution function, such as the equilibrium density profile, $n_b^0 = \int f_b^0 d^3p$, and the determination of the beam boundaries is facilitated by certain transformations of variables, which we now describe.

A point in configuration space, $r, (\theta - k_0 z)$, lies within the beam if the equations which result from the simultaneous vanishing of the arguments of the three delta-functions in the distribution function have a simultaneous solution for real values of the momentum components. For a particular value of $(\theta - k_0 z)$, the beam boundaries $R_b^{\pm}$ are the minimum and maximum values of r for which solutions exist. The argument of the first delta-function, $(C_\perp - \gamma_b^2 m^2 v_0^2)$, subject to the vanishing of that of the third, can be replaced by the quantity $p_\perp^2 + p_\theta^2 + p_z^2 = p_0^2$, where $p_0^2 = [(\gamma_b m v_0^2) + (\gamma_b m V_b)^2]$. This replacement does not change the beam boundaries or the moments of the distribution function. It does simplify the development of expressions for moments of the distribution function and the determination of the beam boundaries. The reason for this is that the equation which results from the vanishing of the modified argument represents a surface in momentum space which is a sphere whose radius is independent of r and $(\theta - k_0 z)$,i.e., the energy-invariant surface. The equation corresponding to the vanishing of the original argument represents a surface in momentum space

which is more complicated and which is a function of $(\theta - k_0 z)$. Accordingly, instead of Eq.(51), we consider the equivalent distribution function

$$f_b^0 = N_s \delta(p^2 - p_0^2)\delta(C_h - C_0)\delta(C_z - C_{z0}), \tag{52}$$

where $p_0^2 = p_r^2 + p_\theta^2 + p_z^2$. The equation which results from the vanishing of the argument, $(C_h - C_0)$, of the second delta-function in Eq.(51) can be expressed as

$$(k_0 r)p_\theta + p_z = k_0 h(r, \theta - k_0 z) \tag{53}$$

where

$$k_o h(r, \theta - k_0 z) = \frac{eB_0}{ck_0}\left[(k_0 r)^2 - (k_0 R_0)^2\right] + \gamma_b m V_b - \frac{e\delta B}{ck_0}(k_0 r)\sin(\theta - k_0 z). \tag{54}$$

This equation represents a surface in momentum space which is a plane. The perpendicular to the plane from the origin lies in the p_θ-p_z plane. Its polar angle from the p_z axis, which we denote by Θ , is given by

$$\Theta = \tan^{-1}\left[1 + (k_0 r)^2\right]^{\frac{1}{2}} \tag{55}$$

where $0 \leq \Theta \leq \pi$. The perpendicular distance of the plane from the origin is a function of r and $(\theta - k_0 z)$. The equation which results from the vanishing of the argument of the third delta function of Eq.(52), $(C_z - C_{z0})$, represents a surface in momentum space which is a right parabolic cylinder. Its generators are perpendicular to the p_z axis. Their direction depends on $(\theta - k_0 z)$.

For a given value of $(\theta - k_0 z)$, the problem of determining the intersection in momentum space is a four-dimensional problem. If r is also specified, it is a three-dimensional problem. The dimensionality of the problem can be reduced to two (or to one if r is specified) by exploiting the geometry of the invariant surfaces in momentum space. The intersection of the three surfaces is equivalent to the intersection of the axial invariant surface (the right parabolic cylinder) with the circle defined by the intersection of the energy invariant surface (the sphere) with the helical invariant surface (the plane). We henceforth refer to this circle as the circle of intersection. A point on the circle of intersection is specified by two variables, r and the azimuthal angle around the circle, which we denote by ϕ'. The intersection of the axial invariant surface with the circle of intersection is described analytically by an equation in the two variables, r and ϕ', which we denote by

$$Q(r, \phi') = 0. \tag{56}$$

These considerations show that the development of expressions for moments of the distribution function and the determination of the beam boundaries will be aided by the use of a rotated cylindrical coordinate system in momentum space. Consider Fig. 4, which shows the energy and helical invariant surfaces and the rotated coordinate system. The cylindrical axis of the rotated coordinate system, $p_{z'}$, lies on the perpendicular from the origin to the helical invariant surface, directed toward it. The cartesian axis $p_{r'}$ coincides with the p_r axis, and the third cartesian axis, $p_{\theta'}$, is chosen so that the set $(p_{r'}, p_{\theta'}, p_{z'})$ forms a right-handed coordinate system. The azimuthal angle ϕ' is measured from the $p_{r'}$ axis. The rotated cylindrical coordinates are $(p_{\perp'}, \phi', p_{z'})$.

We have already stated the dependence of Θ on r in Eq.(55). The rotated cylindrical coordinates of the circle of intersection are $(p_{\perp'0}, \phi', p_{z'0})$, where

$$p_{z'0} = k_0 h[1 + (k_0 r)]^{-\frac{1}{2}}, \tag{57}$$

and

$$p_{\perp'0} = (p_0^2 - p_{z'0}^2)^{\frac{1}{2}}. \tag{58}$$

The transformation between the original and transformed cylindrical coordinates (p_r, ϕ, p_z) and $(p_{r'}, \phi', p_{z'})$ is given by the equations

$$p_r = p_{r'} \tag{59}$$

$$p_\theta = \cos\Theta p_{\theta'} + \sin\Theta p_{z'} \tag{60}$$

$$p_z = -\sin\Theta p_{\theta'} + \cos\Theta p_{z'}. \tag{61}$$

We now use the rotated cylindrical coordinate system to obtain an expression for the equilibrium density profile, $n_b^0 = \int d^3p f_b^0(C_\perp, C_h, C_z)$, for the distribution function in Eq. (52). Note first that the helical invariant surface is described analytically by $p_{z'} = \text{const}$. The argument of the second delta-function is given in the rotated cylindrical coordinate system by

$$C_h - C_0 = k_0^{-1}[1 + (k_0 r)^2]^{\frac{1}{2}}(p_{z'} - p_{z'0}). \tag{62}$$

The argument of the first delta-function can be expressed as $(p^2_{\perp'} - p^2_{\perp'0})$. Thus we obtain

$$f_b^0 = N_s k_0^{-1}[1 + (k_0 r)^2]^{-\frac{1}{2}} \delta(p^2_{\perp'} - p^2_{\perp'0}) \times \delta(p_{z'} - p_{z'0}) \delta(C_z - C_{z0}). \tag{63}$$

The invariant volume element d^3p expressed in terms of the rotated cylindrical coordinate system is $p_{\perp'} dp_{\perp'} d\phi' dp_{z'}$. Introducing the transformed expressions for f_b^0 and d^3p into the definition of n_b^0 and performing the integrations with respect to $p_{\perp'}$ and $p_{z'}$, we obtain

$$n_b^0 = \frac{1}{2} N_s k_0 [1 + (k_0 r)^2]^{-\frac{1}{2}} \times \int_0^{2\pi} d\phi' \delta[\tilde{C}_z(\phi') - C_0]. \tag{64}$$

Here $\tilde{C}_z(\phi)$ denotes the function of $r, (\theta - k_0 z)$ and ϕ' obtained by expressing the axial invariant given in Eq.(6) in terms of the rotated cylindrical coordinate system and introducing the substitutions $p_{\perp'} = p_{\perp'0}$ and $p_{z'} = p_{z'0}$. We represent the delta-function in Eq.(62) in the form

$$\delta[\tilde{C}_z(\phi') - C_0] = \sum_{\{n\}} \frac{\delta(\phi' - \phi'_n)}{\left| \frac{\partial \tilde{C}_z(\phi')}{\partial \phi'} \Big|_{\phi'_n} \right|}, \tag{65}$$

where the sum is over the roots of the equation

$$\tilde{C}_z(\phi') - C_0 = 0. \tag{66}$$

Note that this equation is equivalent to Eq.(56). For points $r, (\theta - k_0 z)$ within the beam, the equation has two roots in the range $0 \leq \phi' \leq 2\pi$. At the beam boundaries there is one root, which corresponds to the tangency of the axial invariant surface (the parabolic cylinder) and the circle of intersection. Outside the beam there are no roots. Finally, performing the integration with respect to ϕ', we obtain

$$n_b^0 = \frac{1}{2} N_s k_0 [1 + (k_0 r)^2]^{-\frac{1}{2}} \times \sum_{\{n\}} \frac{1}{\left| \frac{\partial \tilde{C}_z(\phi')}{\partial \phi'} \Big|_{\phi'_n} \right|}. \tag{67}$$

We now give an explicit expression for $Q(r,\phi')$ [$= \tilde{C}_z(\phi') - C_{z0}$],which is required both for the moments of the distribution function and the beam boundaries. That expression is

$$Q(r,\phi') = \varsigma^2 - \rho^2 + \lambda - \mu, \tag{68}$$

where

$$\varsigma = (\gamma_b m V_b - eB_0/ck_0), \tag{69}$$

$$\rho = \cos\Theta p_{z'0} - \sin\Theta p_{\perp'0}\sin\phi' - eB_0/ck_0, \tag{70}$$

$$\lambda = \frac{2e\delta B}{ck_0}\sin(\theta - k_0 z)(\cos\Theta p_{\perp'0}\sin\phi' + \sin\Theta p_{z'0}), \tag{71}$$

$$\mu = \frac{2e\delta B}{ck_0}\cos(\theta - k_0 z)p_{\perp'0}\cos\phi'. \tag{72}$$

The quantities Θ, $p_{\perp'0}$, and $p_{z'0}$ are given in terms of r and $(\theta - k_0 z)$ by Eqs. (55), (57), and (58).

We now determine the beam boundaries. The most direct method is to search numerically for solutions of Eq.(56) [or, equivalently, Eq.(64)] in the range $0 \leq \phi' \leq 2\pi$ for given values of r, increasing from zero. An alternative method is based on the consideration that the beam boundaries correspond to the tangency of the axial invariant equation with the circle of intersection. Equivalently, the beam boundaries correspond to the tangency of the curve described by $Q(r,\phi')$ as a function of ϕ' with the ϕ' axis. This condition in turn corresponds to the simultaneous solution of Eq.(56) and

$$\frac{\partial}{\partial\phi'}Q(r,\phi') = 0. \tag{73}$$

Numerical solution of this set of equations is required. Newton's method is appropriate. To avoid spurious solutions, it is helpful to calculate first a case far from resonance, for which the approximate analytic expressions for $R_b^{\pm}$ as a function of $(\theta - k_0 z)$ developed by Davidson and Uhm in Ref. 8 are available. Experience has shown that $\phi' \simeq 3\pi/2$ for such cases. We then proceed to the case of interest by gradual evolution of appropriate parameters of the problem with repeated solution of the set of equations, Eqs. (54) and (71). For example, if we are interested in the exact condition of resonance, for which $\omega_c/\omega_0 = 1$, we begin calculations with nominal values of all parameters except ω_c/ω_0. That parameter is initially assigned a value which is sufficiently less than unity that the nonresonant approximation of Ref. 8 is valid.

As a numerical example, in Fig. 5 we show a plot of the normalized radius $k_0 R_b$ of the inner and outer beam envelopes versus $(\theta - k_0 z)$ [from Eqs.(56) and (73)] for the choice of parameters $\delta B/B_0 = 0.01$, $k_0 R_0 = 0.5$, $V_b^2/c^2 = 8/9$, $v_0/c = 0.01$, and $\omega_c/\omega_0 = 0.9$ [Fig. 5(a)], $\omega_c/\omega_0 = 0.915$ [Fig. 5(b)], $\omega_c/\omega_0 = 0.98$ [Fig. 5(c)], and $\omega_c/\omega_0 = 1$ [Fig. 5(d)]. The case $\omega_c/\omega_0 = 0.9$ [Fig. 5(a)] is sufficiently far removed from beam-cyclotron resonance that the results can be modelled approximately by the analytic estimates in Ref. 8. On the other hand, for $\omega_c/\omega_0 = 0.98$ [Fig. 5(c)], the system is sufficiently close to beam-cyclotron resonance that the modulation of the inner- and outer-beam envelopes has grown to large amplitude. Indeed, from Figs. 5(c) and 5(d), the modulation of the inner beam boundary is sufficiently large amplitude that $\partial R_b/\partial(\theta - k_0 z)$ develops a discontinuity at $(\theta - k_0 z) = (2n+1)\pi/2$, $n = 0, \pm 1, \pm 2, ...$, although $R_b(\theta - k_0 z)$ remains continuous. In comparing the curves in Fig. 5 with those in Fig. 2 of Ref. 8, we note that there is a sign error in the latter curves which results from the inclusion [in Eqs.(68) and (69) of Ref. 8] of a minus sign in the first terms of the expressions given for r_b^+ and r_b^-.

We conclude this section by emphasizing that the theoretical analysis developed here can be used to calculate the equilibrium properties of a helically modulated annular electron beam propagating in an equilibrium magnetic field prescribed by Eqs.(1) and (2) without imposing any approximations other than those implicit in the magnetic field configuration assumed.

IV. CONCLUSIONS

This paper extends the development of a self-consistent kinetic description of helically distorted relativistic electron beam equilibria for free electron laser applications to include particular conditions of beam propagation which are of considerable practical interest. Radially confined equilibria are considered for a helically distorted electron beam propagating in the combined transverse wiggler and uniform axial guide fields described by $\boldsymbol{B}^0 = B_0\hat{e}_z + \delta\boldsymbol{B} = B_0\hat{e}_z - \delta B\cos k_0\hat{e}_x - \delta B\sin k_0\hat{e}_z$, where $B_0 = $ const., $\delta B = $ const., and $\lambda_0 = 2\pi/k_0 = $ const. is the axial wavelength of the wiggler field. It is assumed that the beam density and current are sufficiently small that the equilibrium self fields can be neglected in comparison with $\boldsymbol{B}^0$. In this context, it is found that there are three useful (and exact) invariants $(C_\perp, C_h, C_z)$ associated with single-particle motion in the equilibrium field $B_0\hat{e}_z + \delta\boldsymbol{B}$. These invariants are used to construct radially confined Vlasov equilibria $F_b^0(C_\perp, C_h, C_z)$ for an intense relativistic electron beam propagating in the z-direction. Examples of both solid and hollow beam equilibria have been considered (Secs. II and III) and it is shown that the transverse wiggler field can have a large modulational influence on the beam envelope, depending on the size of $\delta B/B_0$. In the present work, no a priori assumption is made that the gyrofrequency $(\omega_c = eB_0/\gamma_b mc)$ of electron motion in the guide field and the frequency of axial electron motion $(\omega_0 = k_0 V_b)$ in the wiggler field are well separated. Thus the condition of beam-cyclotron resonance with $\omega_0 \simeq \omega_c$ can be treated. Numerical procedures for the determination of boundaries of both solid and hollow beam equilibria are developed, and calculations of solid and hollow beam boundaries at resonance are presented in Sec. III.

ACKNOWLEDGMENTS

This research was supported in part by the Office of Naval Research and in part by the Air Force Aeronautical Systems Division.

FIGURE CAPTIONS

Fig.1 Illustrative behavior of $k_0 r(p_z)$ versus p_z [Eq.(41)]: (a) Cutoff behavior at extreme and intermediate values of p_z; (b) Cutoff behavior at extreme values of p_z with two maxima; (c) Cutoff behavior at extreme values of p_z with one maximum.

Fig.2 Illustrative behavior of pseudopotential $U(\eta)$ versus η and corresponding phase space orbits $(\eta, d\eta/d\tau)$ [Eq.(48)] for $\delta B = 0$ in (a), and $\delta B \neq 0$ in (b)–(e). Figures show: (b) Two distinct permitted regions of motion; (c) Boundary between case of two distinct permitted regions of motion and one permitted region of motion; (d) One permitted region of motion, and pseudopotential with two minima; (e) One permitted region of motion, and pseudopotential with one minimum.

Fig.3 Plot of $k_0 R_b$ [Eq.(47)] versus $(\theta - k_0 z)$ for $\delta B/B_0 = 0.01$, $V_b^2/c^2 = 8/9$, $v_0^2/c^2 = 0.02$, $\omega_c/\omega_0 = 0.75$, and (a) $\omega_c/\omega_0 = 0.8$, (b) $\omega_c/\omega_0 = 0.9$, (c) $\omega_c/\omega_0 = 0.95$ and (d) $\omega_c/\omega_0 = 1.0$.

Fig.4 Energy and helical invariant surfaces and rotated coordinate system for annular beam equilibrium.

Fig.5 Plot of normalized radius $k_0 R_b$ of the inner and outer beam envelopes versus $(\theta - k_0 z)$ [Eqs.(56) and (73)] for $\delta B/B_0 = 0.01$, $k_0 R_0 = 0.5$, $V_b^2/c^2 = 8/9$, $v_0/c = 0.01$, and (a)$\omega_c/\omega_0 = 0.9$, (b)$\omega_c/\omega_0 = 0.915$, (c)$\omega_c/\omega_0 = 0.98$ and (d)$\omega_c/\omega_0 = 1.0$.

REFERENCES

1 H.P. Freund, P. Sprangle, D. Dillenburg, E.H. da Jornada, B. Liberman, and R.S. Schneider, Phys. Rev. A *24*, 1965 (1981).

2 T. Kwan and J.M. Dawson, Phys. Fluids *22*, 1089(1979).

3 R.C. Davidson and H.S. Uhm, Phys. Fluids *23*, 2076 (1980).

4 I.B. Bernstein and J.L. Hirshfield, Phys. Rev. A *20*, 1661 (1979); L. Friedland, Phys. Fluids *23*, 2376 (1980).

5 P. Sprangle and R.A. Smith, Phys. Rev. A *21*, 293 (1980).

6 T.C. Marshall, S. Talmadge, and P. Efthimion, Appl. Phys. Lett. *31*, 320 (1977).

7 D.A.G. Deacon, L.R. Elias, J.M.M. Madey, G.J. Ramian, H.A. Schwettman, and T.I. Smith, Phys. Rev. Lett *38*, 897 (1977).

8 R.C. Davidson and H.S. Uhm, J. Appl. Phys. *53*, 2910 (1982).

9 W.A. McMullin and R.C. Davidson, Phys. Rev. A *25*, 3130 (1982).

10 V.P. Sukhatme and P.A. Wolff, J. Appl. Phys. *44*, 2331 (1973).

11 W.B. Colson, Phys. Lett. *59A*, 187 (1976).

12 N.M. Kroll and W.A. McMullin, Phys. Rev. A *17*, 300 (1978).

13 F.A. Hopf, P. Meystre, M.O. Scully and W.H. Louisell, Opt. Commun. *18*, 413 (1976).

14 P. Sprangle and R.A. Smith, Phys. Rev. A *21*, 293 (1980).

15 R.C. Davidson, *Theory of Nonneutral Plasmas* (Benjamin, Reading, Massachusetts, 1974).

16 H.P. Freund and A.T. Drobot, Phys. Fluids *25*, 736 (1982).

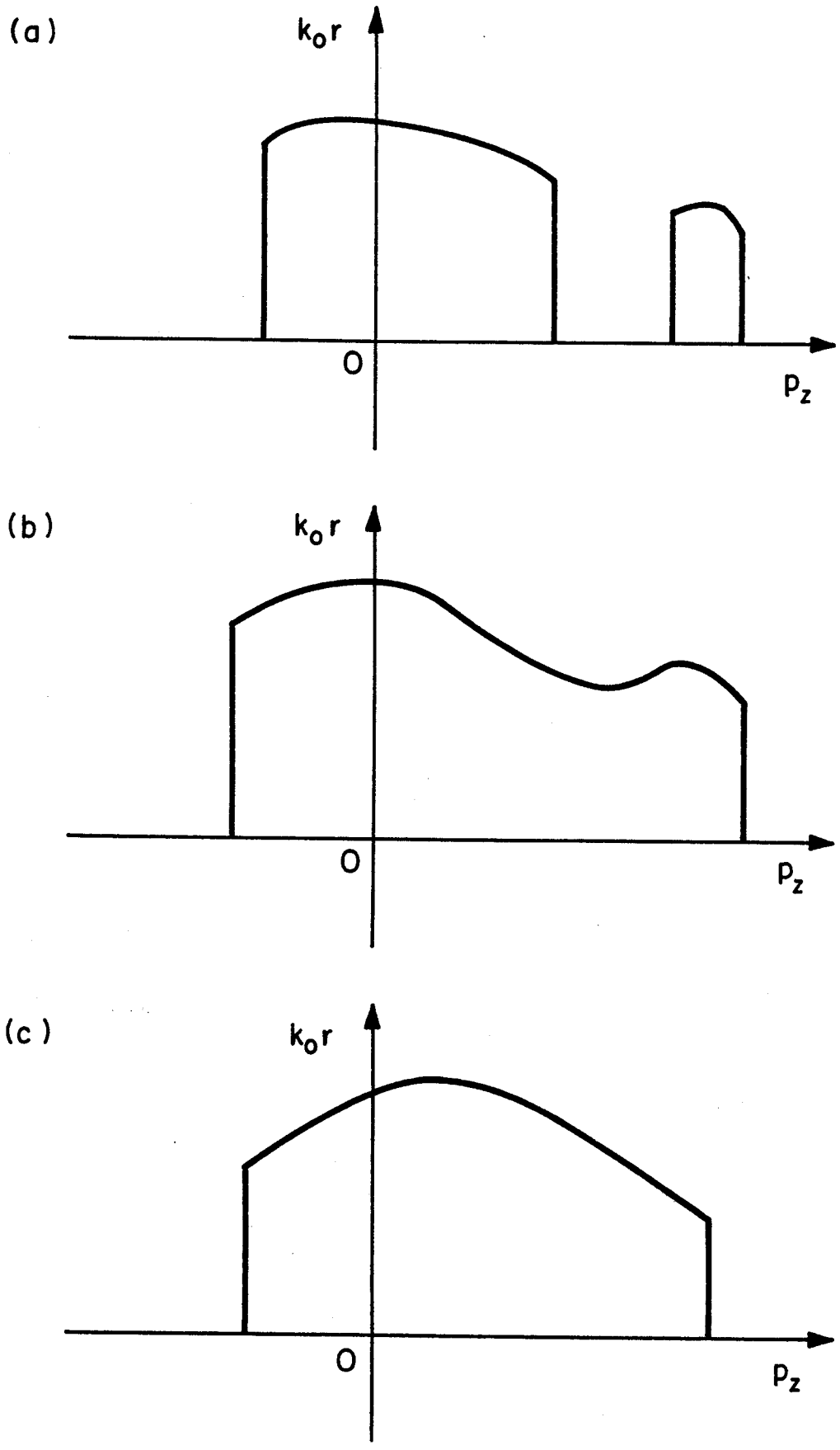

Fig. 1

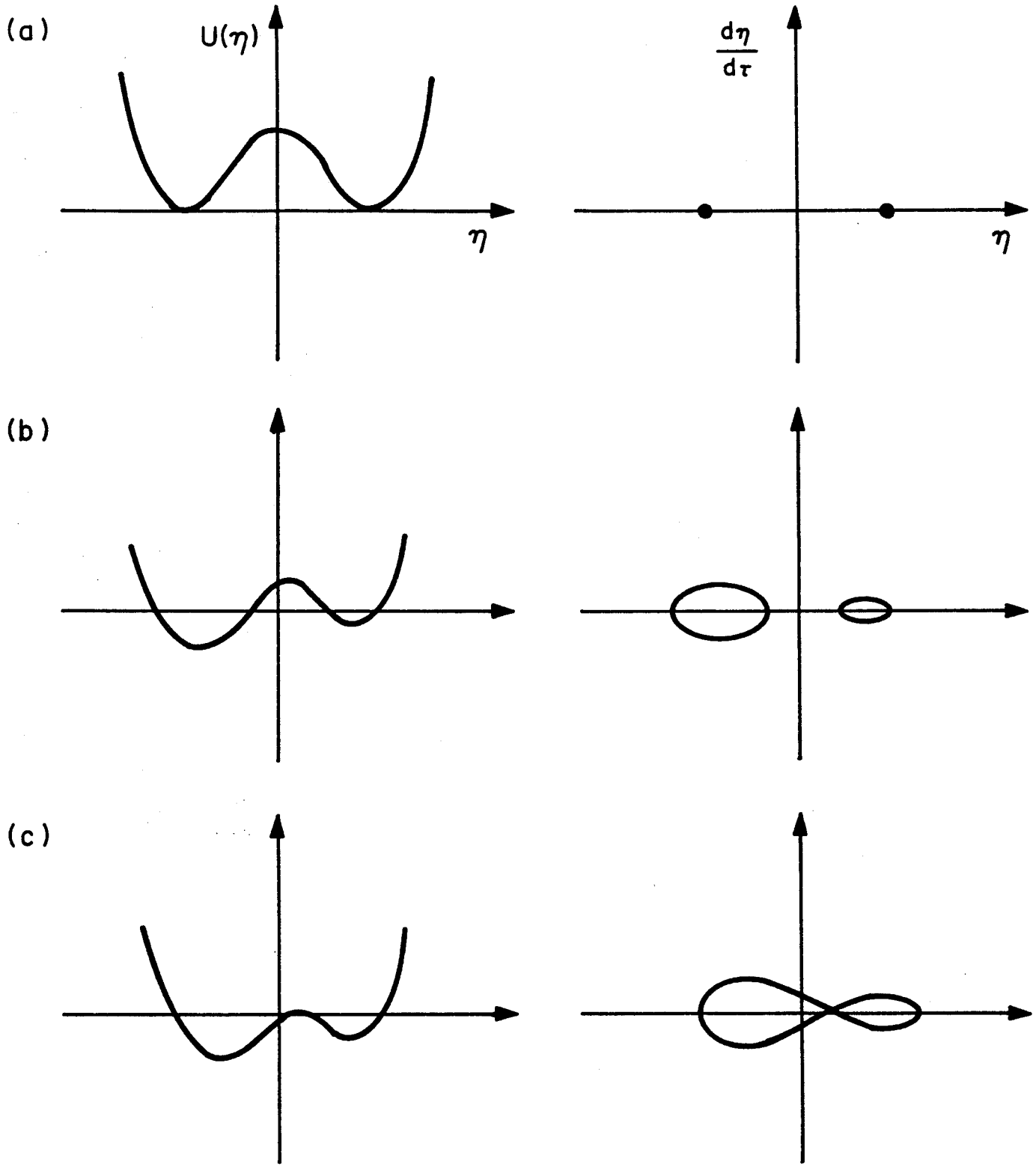

Fig. 2

(d)

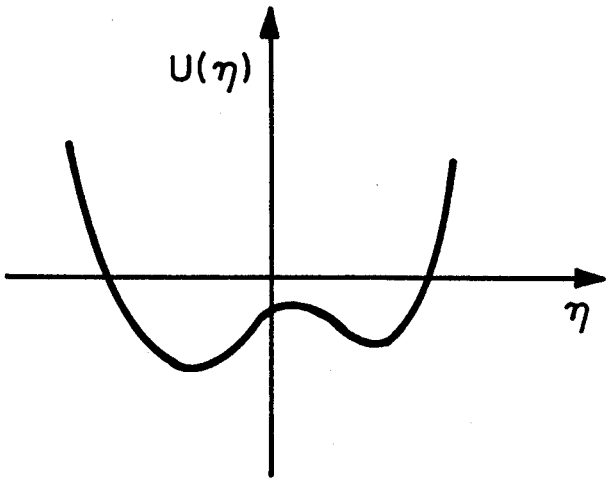

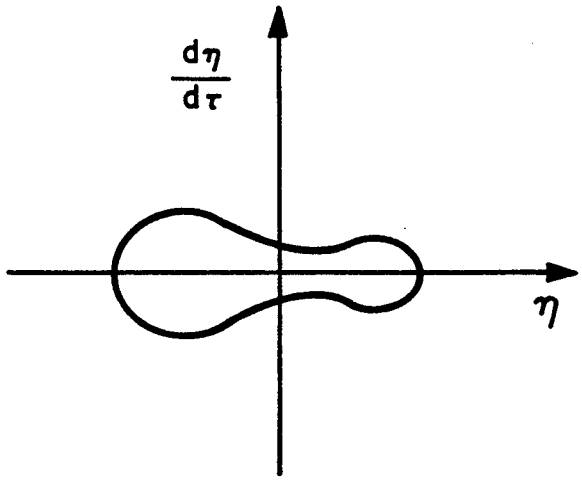

(e)

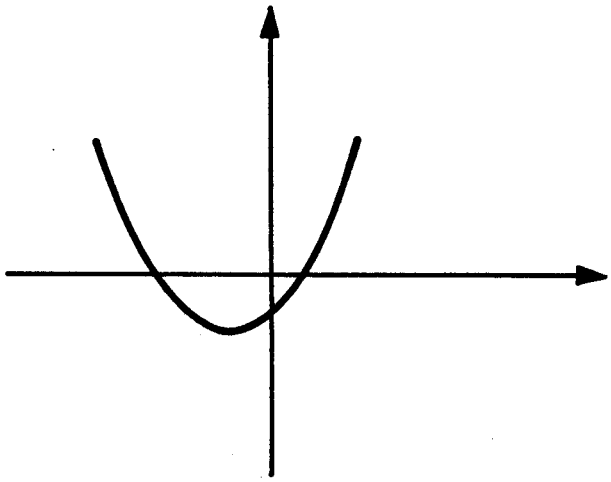

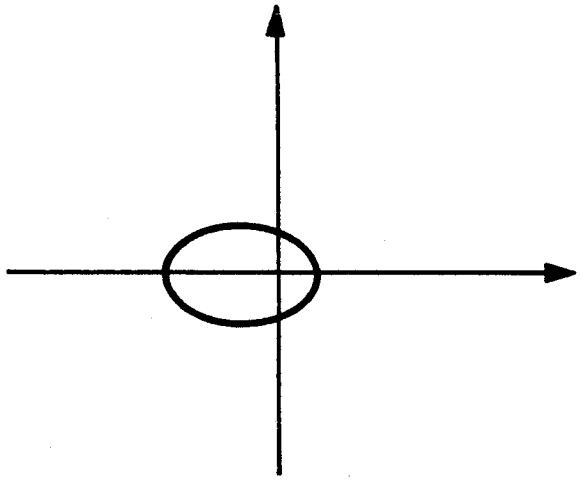

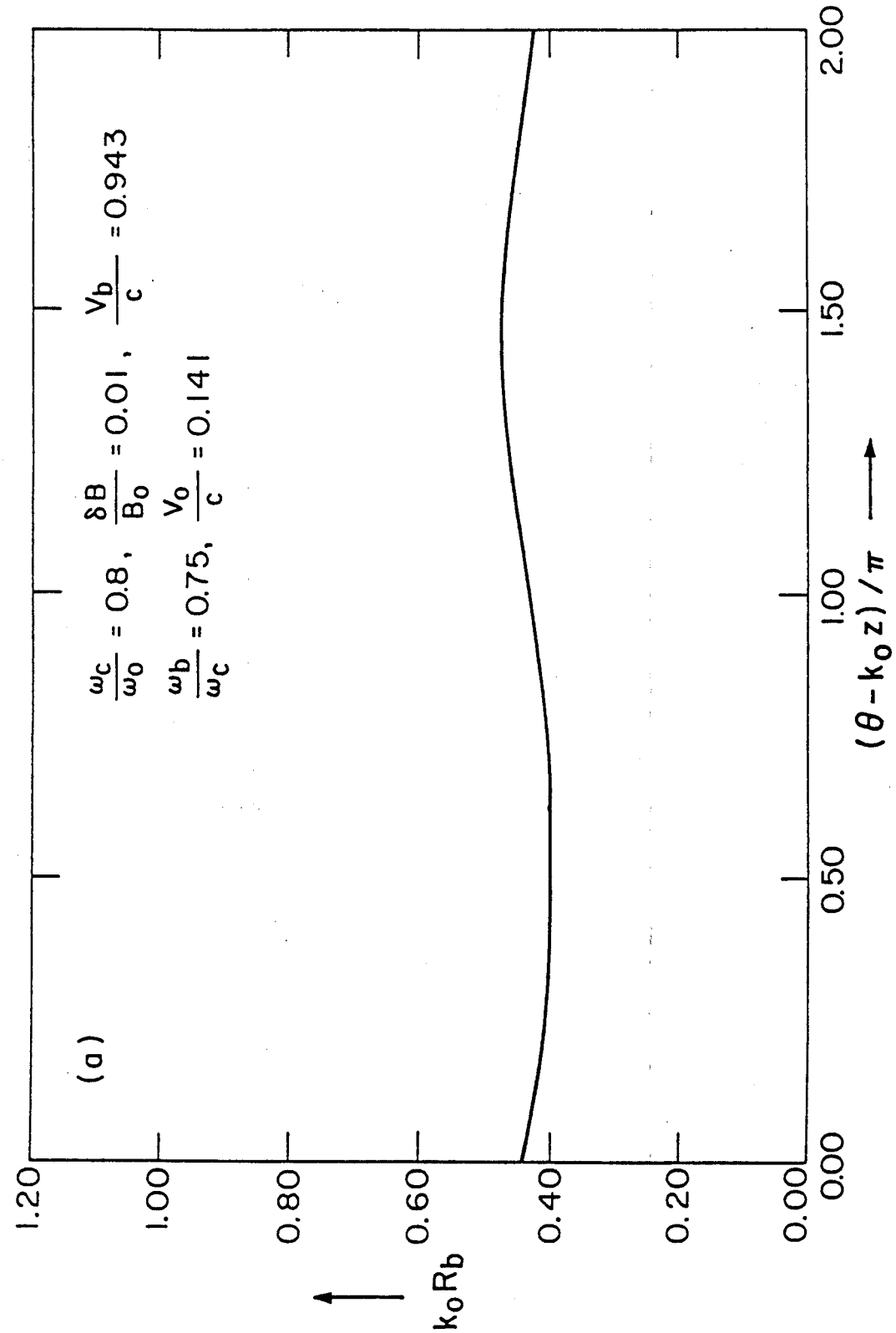
(a)
$\frac{\omega_c}{\omega_o} = 0.8$, $\frac{\delta B}{B_o} = 0.01$, $\frac{V_b}{c} = 0.943$
$\frac{\omega_b}{\omega_c} = 0.75$, $\frac{V_o}{c} = 0.141$
$k_o R_b$
$(\theta - k_o z)/\pi$
1.20
1.00
0.80
0.60
0.40
0.20
0.00
0.00
0.50
1.00
1.50
2.00

Fig. 3(a)

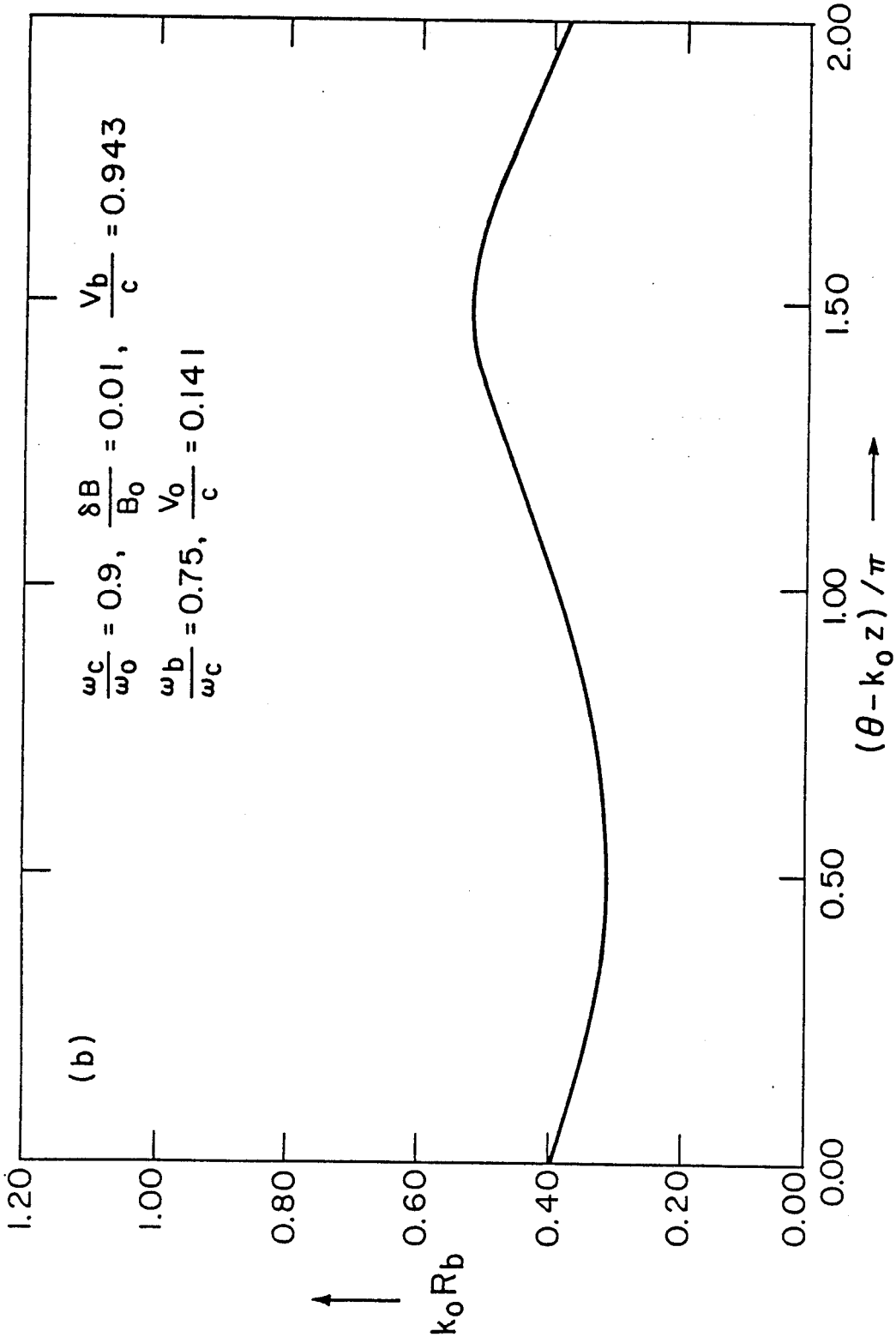
(b)
$\frac{\omega_c}{\omega_o} = 0.9, \quad \frac{\delta B}{B_o} = 0.01, \quad \frac{V_b}{c} = 0.943$
$\frac{\omega_b}{\omega_c} = 0.75, \quad \frac{V_o}{c} = 0.141$
$k_o R_b$
$(\theta - k_o z)/\pi$
0.00
0.20
0.40
0.60
0.80
1.00
1.20
0.50
1.00
1.50
2.00

Fig. 3(b)

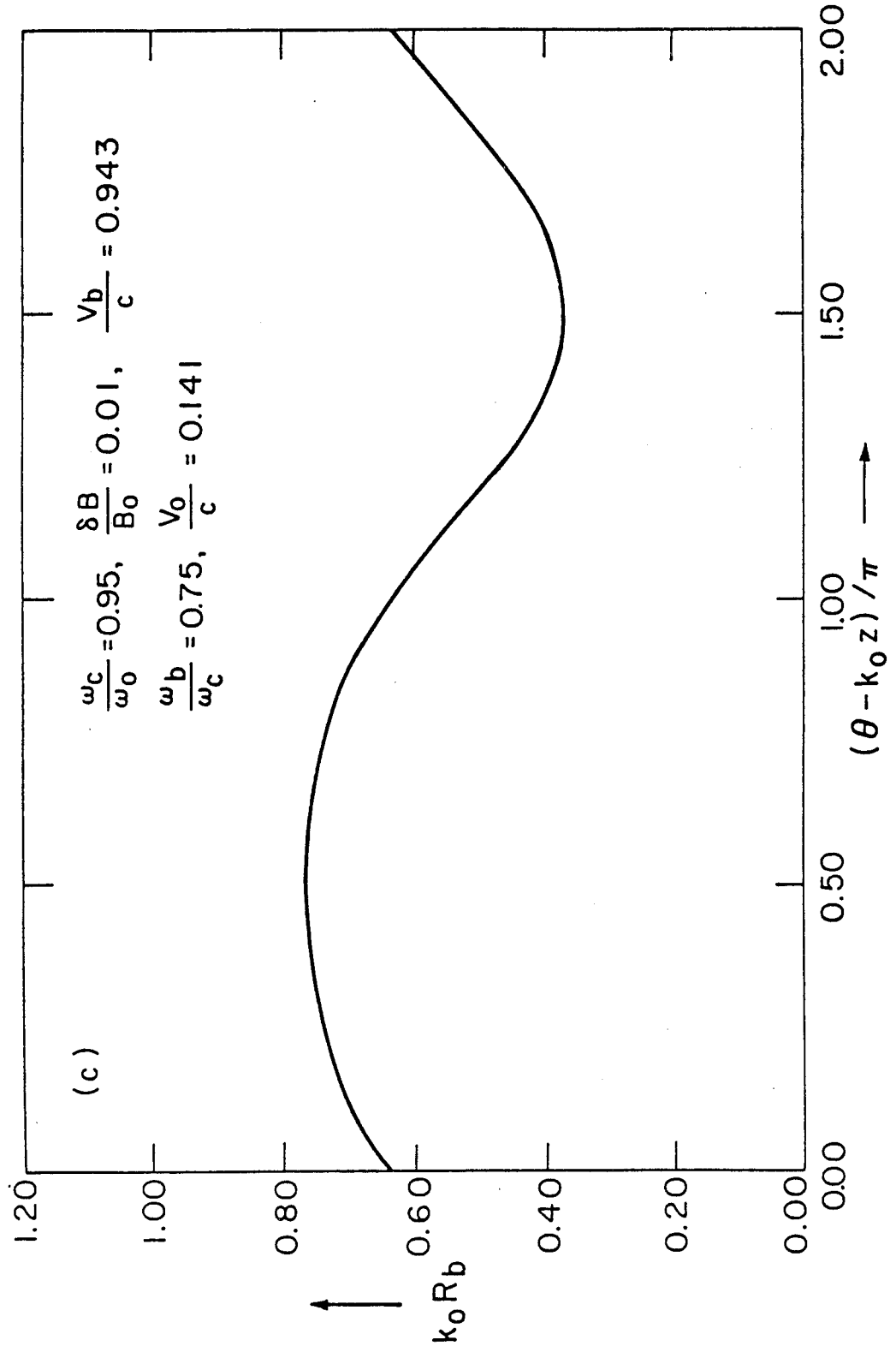
(c)
$\frac{\omega_c}{\omega_o}$ =0.95, $\frac{\delta B}{B_o}$ =0.01, $\frac{V_b}{c}$ = 0.943
$\frac{\omega_b}{\omega_c}$ =0.75, $\frac{V_o}{c}$ = 0.141
$k_o R_b$
$(\theta - k_o z)/\pi$
0.00
0.20
0.40
0.60
0.80
1.00
1.20
0.50
1.00
1.50
2.00

Fig. 3(c)

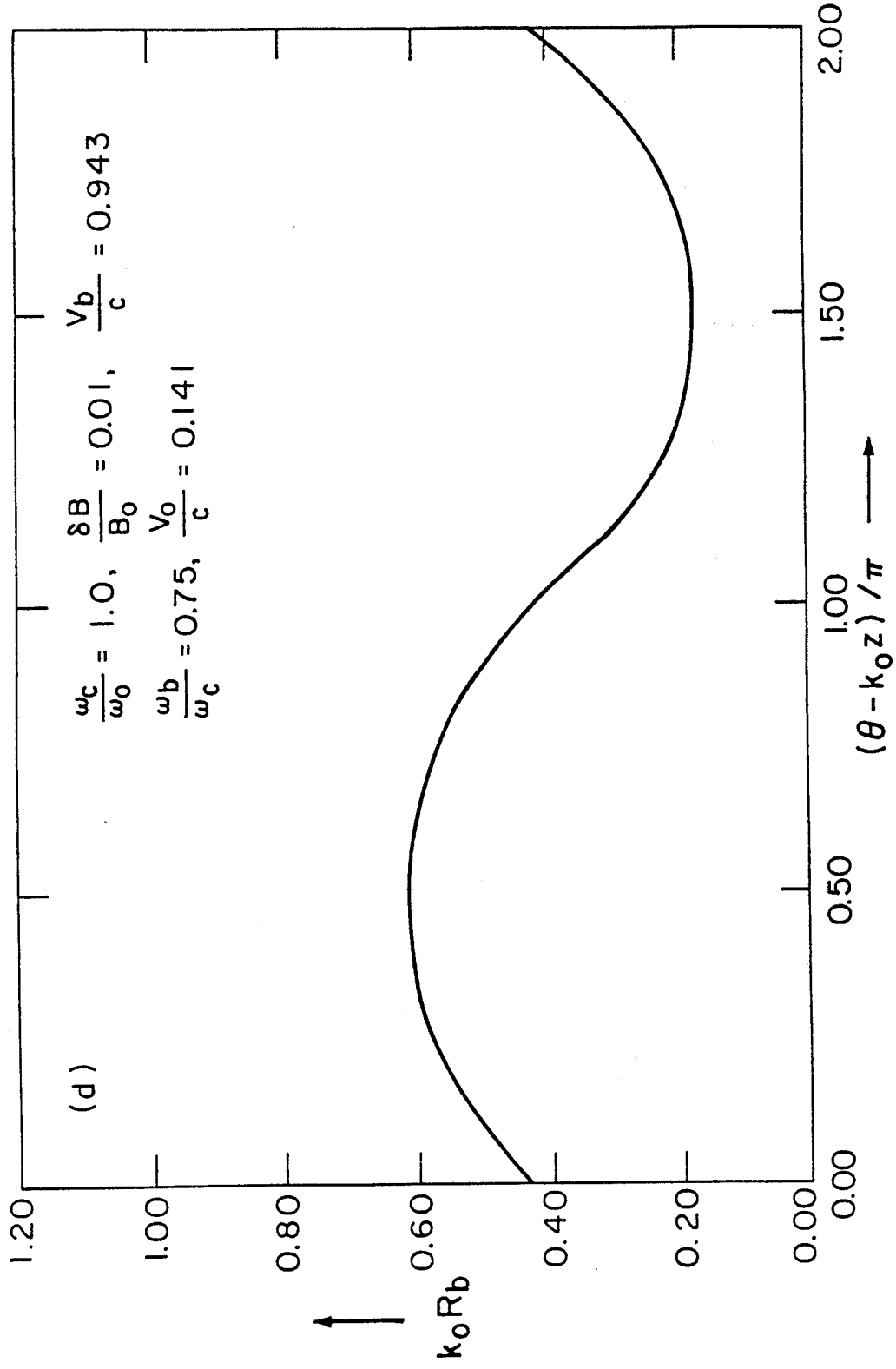
(d)
$\frac{\omega_c}{\omega_o} = 1.0$, $\frac{\delta B}{B_o} = 0.01$, $\frac{V_b}{c} = 0.943$
$\frac{\omega_b}{\omega_c} = 0.75$, $\frac{V_o}{c} = 0.141$
$k_o R_b$
$(\theta - k_o z)/\pi$
0.00
0.20
0.40
0.60
0.80
1.00
1.20
0.00
0.50
1.00
1.50
2.00

Fig. 3(d)

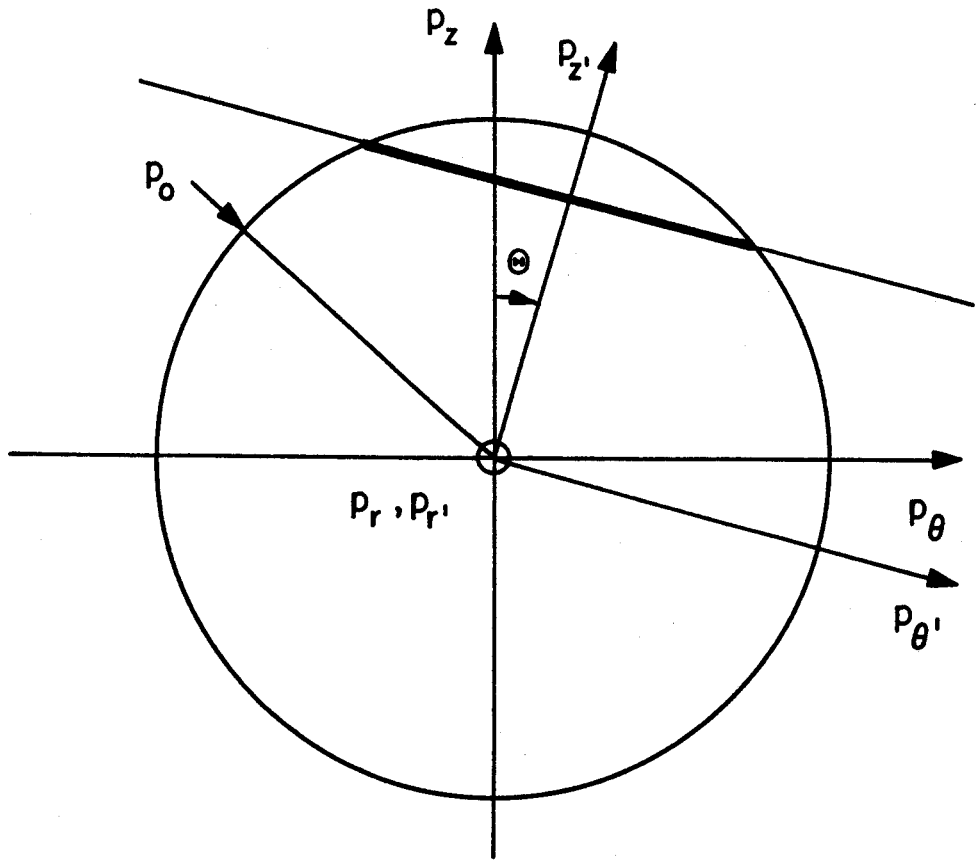

Fig. 4

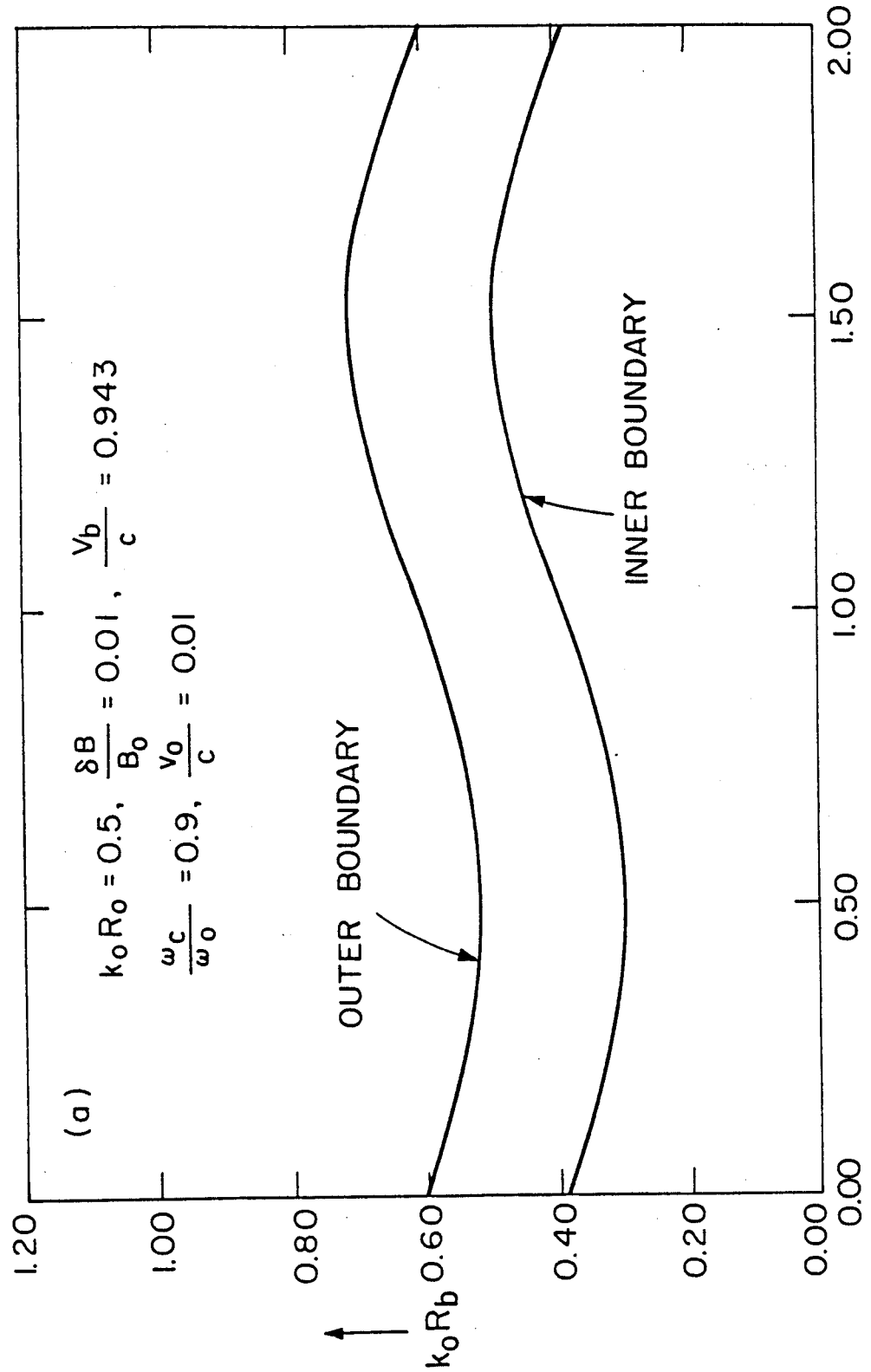
(a)
$k_o R_o = 0.5$, $\frac{\delta B}{B_o} = 0.01$, $\frac{v_b}{c} = 0.943$
$\frac{\omega_c}{\omega_o} = 0.9$, $\frac{v_o}{c} = 0.01$
OUTER BOUNDARY
INNER BOUNDARY
$k_o R_b$
$(\theta - k_o z)/\pi$
1.20
1.00
0.80
0.60
0.40
0.20
0.00
0.00
0.50
1.00
1.50
2.00

Fig. 5(a)

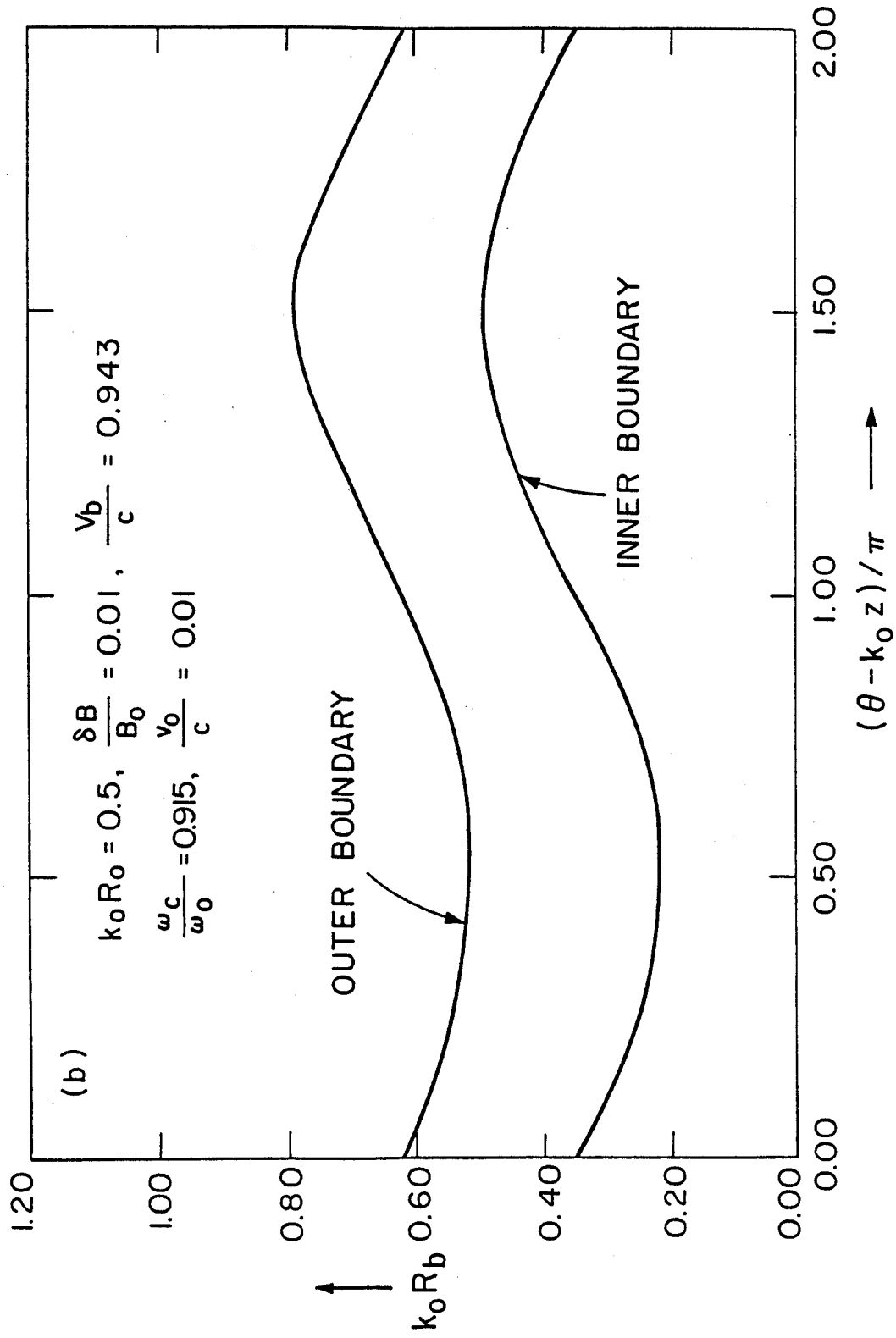
(b)
$k_0R_0 = 0.5$, $\frac{\delta B}{B_0} = 0.01$, $\frac{v_b}{c} = 0.943$
$\frac{\omega_c}{\omega_0} = 0.915$, $\frac{v_0}{c} = 0.01$
OUTER BOUNDARY
INNER BOUNDARY
k_0R_b
$(\theta - k_0 z)/\pi$
1.20
1.00
0.80
0.60
0.40
0.20
0.00
0.00
0.50
1.00
1.50
2.00

Fig. 5(b)

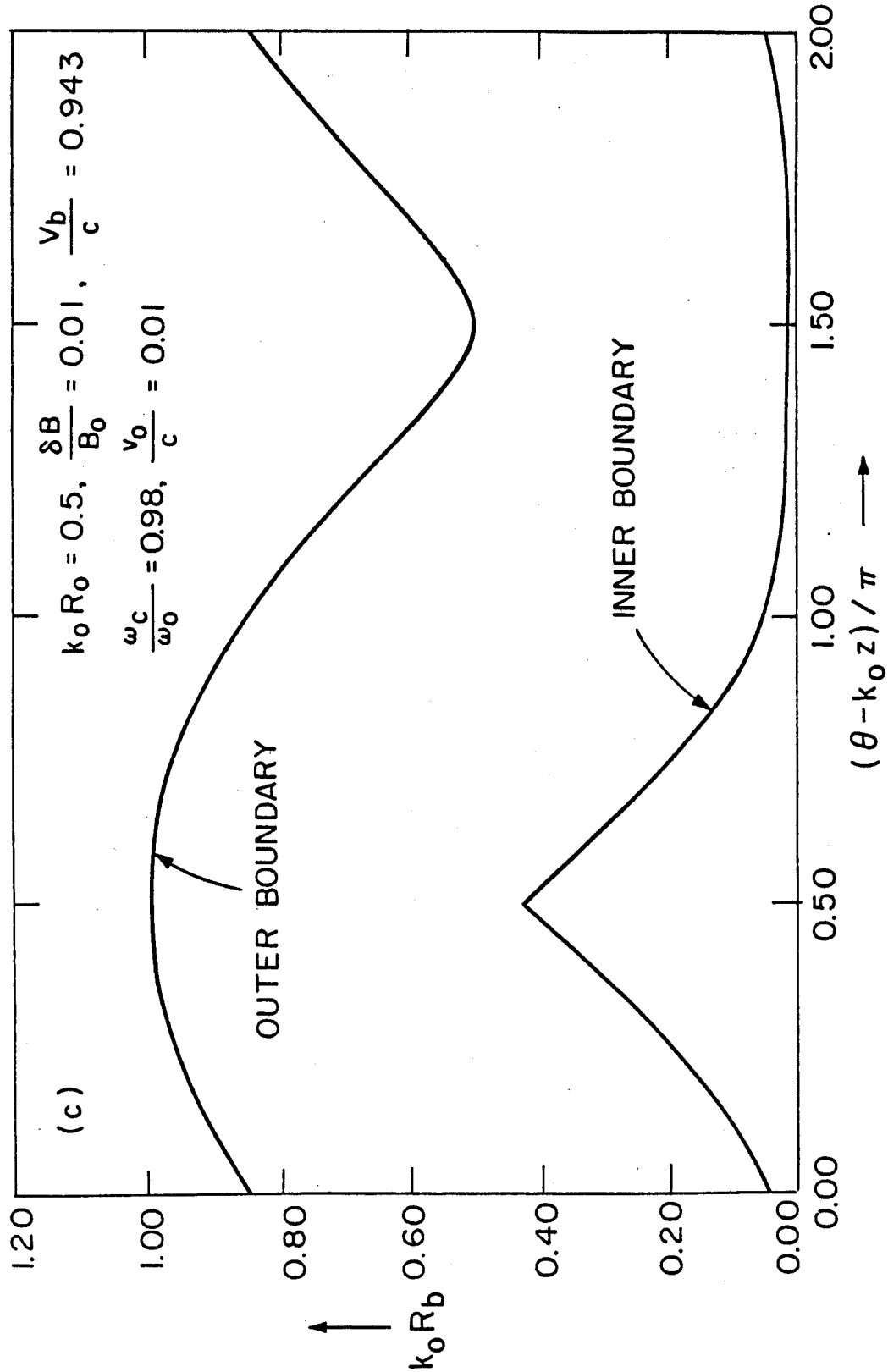
(c)
$k_o R_o = 0.5$, $\frac{\delta B}{B_o} = 0.01$, $\frac{V_b}{c} = 0.943$
$\frac{\omega_c}{\omega_o} = 0.98$, $\frac{v_o}{c} = 0.01$
OUTER BOUNDARY
INNER BOUNDARY
$k_o R_b$
$(\theta - k_o z)/\pi$
1.20
1.00
0.80
0.60
0.40
0.20
0.00
0.00
0.50
1.00
1.50
2.00

Fig. 5(c)

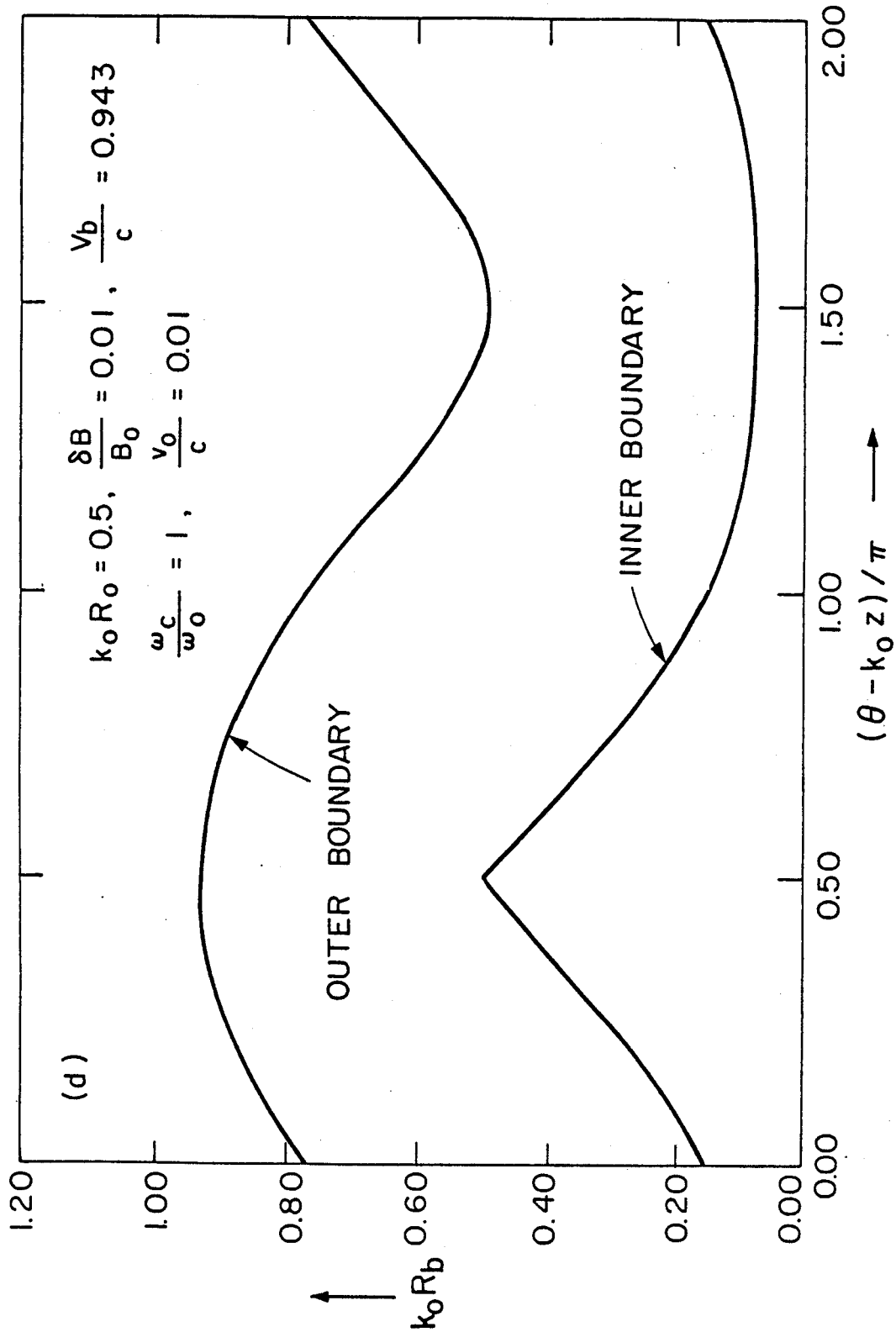
(d)
$k_o R_o = 0.5$, $\frac{\delta B}{B_o} = 0.01$, $\frac{v_b}{c} = 0.943$
$\frac{\omega_c}{\omega_o} = 1$, $\frac{v_o}{c} = 0.01$
OUTER BOUNDARY
INNER BOUNDARY
$k_o R_b$
$(\theta - k_o z)/\pi$
1.20
1.00
0.80
0.60
0.40
0.20
0.00
0.00
0.50
1.00
1.50
2.00

Fig. 5(d)